NPS-63-81-004

NAVAL POSTGRADUATE SCHOOL

Monterey, California

A Review and Evaluation of Integrated Atmospheric Boundary - Layer Models for Maritime Applications

C.W. Fairall, K.L. Davidson and G.E. Schacher

Environmental Physics Group
Naval Postgraduate School
Monterey, CA 93940

November 1981

Prepared for:
Naval Air Systems Command
(Air 3701)
Washington, D.C. 20360

NAVAL POSTGRADUATE SCHOOL
Monterey, California

Rear Admiral J.J. Ekelund
Superintendent

David A. Schrady
Acting Provost

The work reported herein was supported in part by the Naval Air Systems Command, (Air 3701), Washington, D.C. 20360.

This report was prepared by:

UNCLASSIFIED

SECURITY CLASSIFICATION OF THIS PAGE (When Date Entered)

REPORT DOCUMENTATION PAGE		READ INSTRUCTIONS BEFORE COMPLETING FORM
1. REPORT NUMBER NPS-63-81-004	2. GOVT ACCESSION NO.	3. RECIPIENT'S CATALOG NUMBER
4. TITLE (and Subtitle) A Review and Evaluation of Integrated Atmospheric Boundary - Layer Models for Maritime Applications		5. TYPE OF REPORT & PERIOD COVERED Technical Report 6. PERFORMING ORG. REPORT NUMBER
7. AUTHOR(s) C.W. Fairall, K.L. Davidson and G.E. Schacher		8. CONTRACT OR GRANT NUMBER(s)
9. PERFORMING ORGANIZATION NAME AND ADDRESS Physics and Chemistry Department Naval Postgraduate School Monterey, CA 93940		10. PROGRAM ELEMENT, PROJECT, TASK AREA & WORK UNIT NUMBERS 61153N;A370370G/186A/1R033-02-001 N0001081WR11104
11. CONTROLLING OFFICE NAME AND ADDRESS Naval Air Systems Command (Air 3701) Washington, D.C. 20360		12. REPORT DATE November 1981 13. NUMBER OF PAGES 89
14. MONITORING AGENCY NAME & ADDRESS(if different from Controlling Office)		15. SECURITY CLASS. (of this report) Unclassified 15a. DECLASSIFICATION/DOWNGRADING SCHEDULE

16. DISTRIBUTION STATEMENT (of this Report)

Distribution Unlimited

17. DISTRIBUTION STATEMENT (of the abstract entered in Block 20, if different from Report)

18. SUPPLEMENTARY NOTES

C.W. Fairall is an employee of the BDM Corporation.

19. KEY WORDS (Continue on reverse side if necessary and identify by block number)

Marine Boundary Layer, Boundary Layer Modeling, Environmental Effects on Naval Systems

20. ABSTRACT (Continue on reverse side if necessary and identify by block number)

This work is an examination of the state-of-the-art of the two layer, integrated type atmospheric mixed-layer models with emphasis on applications to the marine regime. A linear synoptic scale mixed-layer microphysical scale model structure is suggested for short term (24 hour) forecasts of atmospheric variables with naval applications. Several potential deficiencies in the present knowledge are identified for physical parameterizations (particularly the entrainment rate) and the synoptic scale forcing requirements. It is concluded that these models, though promising, have not been verified for a

DD FORM 1 JAN 73 1473 EDITION OF 1 NOV 65 IS OBSOLETE
S/N 0102-014-6601

UNCLASSIFIED

SECURITY CLASSIFICATION OF THIS PAGE (When Date Entered)

20. wide range of atmospheric conditions.

CONTENTS

ABSTRACT

This work is an examination of the state-of-the-art of the two layer, integrated type atmospheric mixed-layer models with emphasis on applications to the marine regime. A linked synoptic scale mixed-layer microphysical scale model structure is suggested for short term (24 hour) forecasts of atmospheric variables with naval applications. Several potential deficiencies in the present knowledge are identified for physical parameterizations (particularly the entrainment rate) and the synoptic scale forcing requirements. It is concluded that these models, though promising, have not been verified for a wide range of atmospheric conditions.

I. SUMMARY

A. INTRODUCTION

It is clear that boundary layer models hold great potential for extending and expanding local atmospheric assessments. The integrated type mixed layer model is one obvious candidate for this application, particularly over the ocean. Second order closure models are also likely candidates, but because of their much greater computer requirements, they will probably be operational somewhat further in the future. The integrated model employs rate equations for the mean quantities only, assumes linear vertical flux profiles and obtains entrainment rates and turbulence by empirical methods. The second order closure models are considerably more complex. Since our own area of expertise is with the integrated model, we shall not discuss second order closure further.

The central text of this paper is an exploration of the state-of-the-art for mixed layer models with a focus on the sources of uncertainty and areas needing development. We will also discuss, somewhat more briefly, the present situation in obtaining operational output and problems associated with actually implementing a field version of this model.

B. CONCLUSIONS

Barring some very extensive breakthroughs in satellite remote sensing technology, local measurements (such as radiosondes) and meteorological observations will be required to provide a spectrum of information of atmospheric effects on Naval operations. Extending these measurements through 6-to-24 hour forecasts will

probably require on-board computer based atmospheric models supported by large scale numerical field models with regional window capability (for example, the US Navy NORAPS system). The two or three layer integrated type marine mixed layer model is a very good choice for these local assessments because it is ideally suited to the good horizontal homogeneity and near dynamic equilibrium situations that often characterize the open ocean. Thus, the synoptic scale model, the local data, the integrated boundary layer model and the operational output parameterization could be linked together to produce local boundary layer forecasts. A sample flow diagram for such a system is given in Fig. 1.

The feasibility of a linked synoptic-boundary layer-micrometeorology model is primarily dependent upon three issues: 1) can a synoptic scale model (with regional resolution) provide sufficiently accurate forecasts of the synoptic forcing, 2) given accurate synoptic forcing, can the integrated model provide sufficiently accurate forecasts of the boundary layer evolutions and 3) can the relevant operation information be extracted from the mixed layer model structure? This paper will concentrate on question two, with a brief background on the third question. The first question is beyond the area of expertise of the authors of this paper although we have examined certain alternatives to the synoptic scale model (namely, single station assessment techniques).

The following conclusions will be discussed in the examination of the mixed layer model:

1) The basic model structure is obtained from simple boundary layer averages of conservative (or near conservative) quantities. The evolution of the boundary layer is then predicted from rate equations derived from the conservative expression. There are a few special cases to consider (temperature and mean wind), but in principle the model structure is extremely simple.

2) The internal structure of the model requires the parameterization of certain boundary layer energy transfer processes. These parameterizations are in fairly good shape for surface fluxes, cloud microphysics and radiative flux interactions. There is still some work to be done in these areas, but most of the questions will probably be resolved within the next few years. Conversely, the entrainment parameterizations are not adequate to handle several well known entrainment mechanisms (inversion wind shear, cloud top instability or atmospheric wave phenomena, for example). Since inversion wind shear conditions are common, this particular process needs further investigation.

3) The synoptic and mesoscale effects (subsidence and advection) are often as important as entrainment. Synoptic scale numerical models are very important here because not only can they provide the relevant data, but also they are sources of <u>forecasts</u> of synoptic scale forcing. Whether the present (or near future) models will be adequate has not been determined. The mesoscale gradient method (using satellite remote sensed data perhaps) and

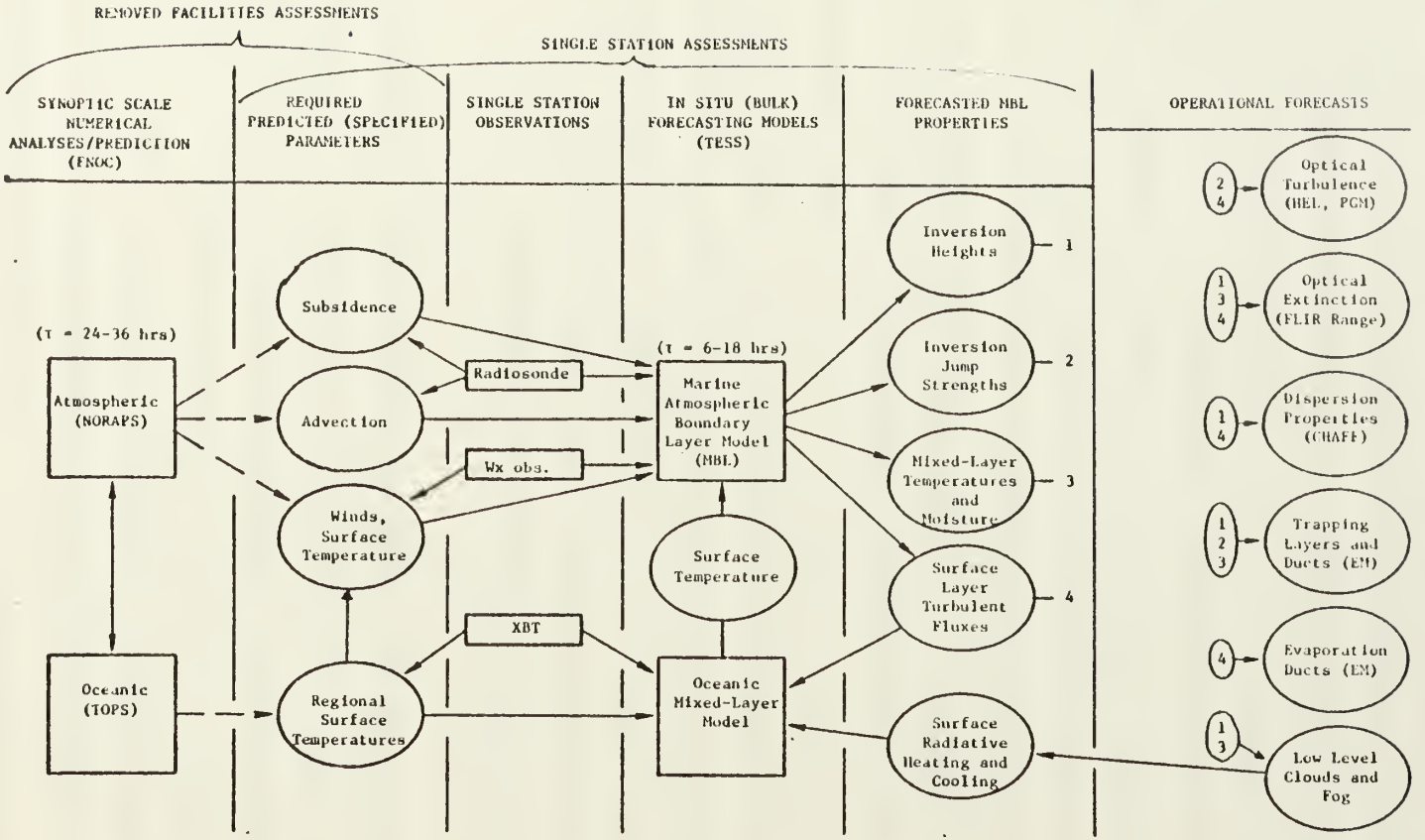

Figure 1. Block diagram of coupled large scale and boundary layer models for the atmosphere and ocean.

single station methods may be able to provide "nowcasts" of certain synoptic terms. For example, the sea-surface temperature field will almost certainly be required to use the model successfully. The single station rawindsonde can provide local values of subsidence and thermal advection but the accuracy is marginal. In short, the required large scale forcing for a complete model application is questionable.

4) The algorithms required to extract operational variables from mixed layer parameters are in an advanced state of development. There are some problems remaining (continental aerosols, for example) but it is our judgement that most of the bulk atmospheric characterizations are now available to reasonable accuracy.

5) The full model structure as defined in Fig. 1 is completely unverified. The boundary layer model has only been successfully verified on a few selected sets of atmospheric data. Of course, most of the individual components of the model can be verified separately. For example, a candidate radiation flux profile parameterization can be tested against measured radiation profiles without being concerned with the evolution of the boundary layer. Assuming that reasonably accurate boundary layer expressions and large scale forcing data are used, then testing the model against data is basically a verification of the model simplifying assumptions and the particular entrainment parameterization chosen by the researcher. A comprehensive study of the accuracy of the boundary layer model over a wide range of marine atmospheric conditions has yet to be performed.

II. MODEL BACKGROUND

Boundary layer models consider two basic atmospheric regions the boundary layer ($Z<h$ where Z is the height above the surface) and the free atmosphere ($Z>h$) separated by a thin transition region at height, h. The boundary layer is turbulent while the free atmosphere is relatively non-turbulent. The boundary layer can be thought of as an interaction region between two large masses - the ocean and the free atmosphere. The boundary layer interacts with the ocean at the sea surface and with the free atmosphere at the transition zone (usually referred to as the inversion). Because of the strong turbulence in the boundary layer, it is quite homogeneously mixed vertically (thus the terminology "well-mixed" and "mixed-layer").

The well-mixed nature of the boundary layer implies that certain meteorological variables are height independent for $Z<h$. For example, the water vapor mixing ratio, $q = Q/\rho$, where Q is th density of atmospheric water vapor and ρ is the density of air (Fig. 2). Thus , we assert that any well-mixed meteorological varable, ϕ , can be represented as

$$\phi(Z) = \phi_m \qquad Z<h \qquad (1a)$$

$$\phi(Z) = \phi_m + \Delta\phi + \Gamma_\phi(Z-h) \qquad Z>h \qquad (1b)$$

where ϕ_m is the well-mixed value, $\Delta\phi$ is the "jump" at the inversion and Γ_ϕ is the mean vertical gradient of ϕ (assumed zero for $Z<h$) in the free atmosphere. The height dependent variable, $\phi(Z)$, is now reduced to three parameters: ϕ_m, $\Delta\phi$ and Γ_ϕ . This is known as a "zero-order" model since we allow a discontinuity a the inversion. The purpose of the model is simply to predict the time evolution of these three parameters for each variable of

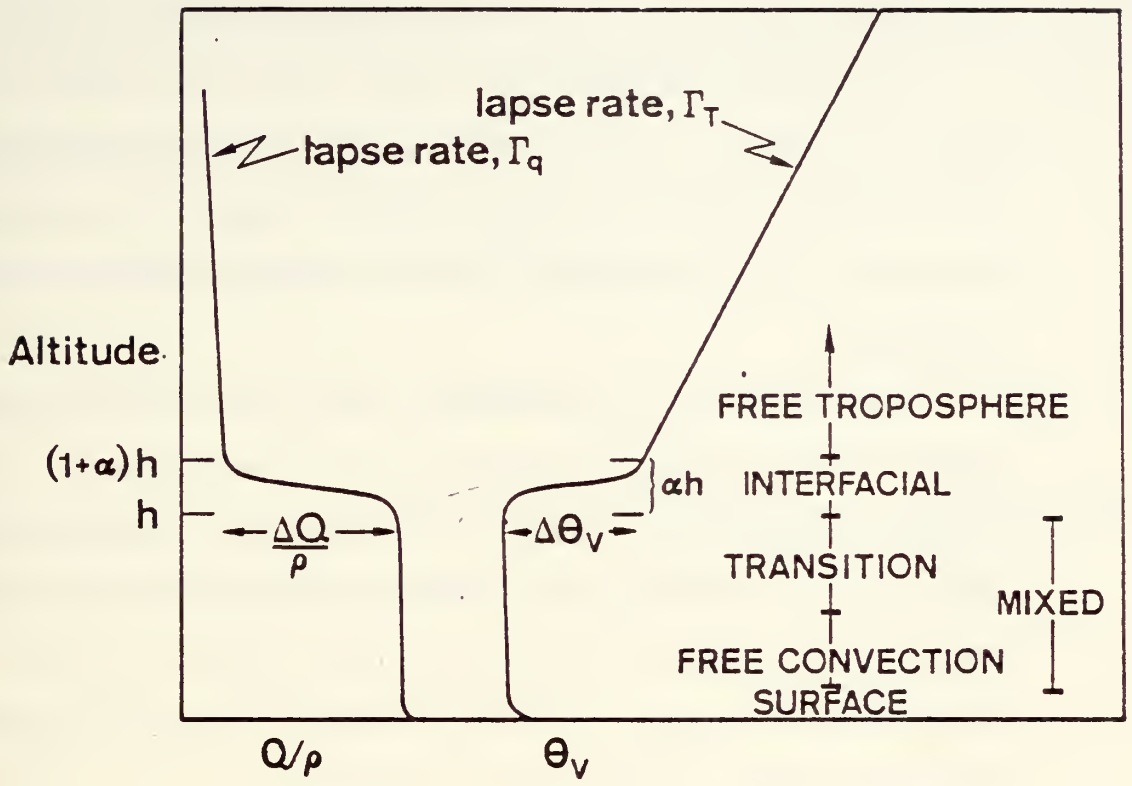

Figure 2. Schematic representation of the two layer model structure for clear sky conserved atmospheric variables-water vapor mixing ratio, Q/ρ, and virtual potential temperature, θ_v. The height of the well-mixed layer is h capped by an inversion of thickness αh.

interest and relate these parameters to quantities of direct operational relevance. The basic method is to relate ϕ at some time, t, ($\phi(t)$) to an initial value, ϕi, through the rate equation, $d\phi/dt$, for a small time step $t - t_i$,

$$\phi(t) = \phi i + (d\phi/dt)\ (t - t_i) \qquad (2)$$

The rate equations are relationships of $d\phi/dt$ to the physical processes in the atmosphere. For the boundary layer, the major processes are interactions with the surface and the free atmosphere.

Interaction of the boundary layer air with the ocean surface is the primary source of boundary layer turbulence. (Note, however, that cloud radiative cooling and inversion wind shear ca also generate turbulence.) The free atmosphere is effectively "cut-off" from this turbulence by the inversion zone. The interaction with the surface is characterized by surface fluxes o momentum (wind), sensible heat (temperature) and latent heat of evaporation (water vapor). Since the fluxes are essentially zero for Z>h, they must vary with height within the boundary layer. I other words, the vertical flux of the quantity ϕ, designated $F_\phi(Z)$, is function of Z. The height dependence of F_ϕ is a critical factor in the temporal evolution of $\phi(Z)$. For a conservative quantity, the rate of change of ϕ with time due to the flux is equal to the vertical gradient of the flux

$$d\phi/dt = - dF_\phi(Z)/dZ \qquad (3)$$

The well-mixed assumption ($d\phi/dZ = 0$) in the boundary layer is therefore equivalent to assuming that $dF_\phi(Z)/dZ$ is constant, or that $F_\phi(Z)$ has a linear height dependence.

Equation 3 applies to changes in the atmospheric reference frame (Lagrangian). If we consider ϕ at a point fixed above the earth's surface (rather than a point that translates with the atmospheric motion), then we must account for the possibility that ϕ may change with time due to horizontal gradients in ϕ. If we define the mean horizontal wind vector, $\vec{U}$, the horizontal gradient, ∇_H , the mean vertical air velocity, $\overline{w}$ and the vertical gradient of ϕ, $d\phi/dZ$, then

$$d\phi/dt \rightarrow d\phi/dt + \vec{U}\cdot\nabla_H\phi + \overline{w}\, d\phi/dZ \qquad (4)$$

The horizontal term is referred to as "advection" and the vertical term is referred to as "subsidence". Thus, the equation

$$d\phi/dt = -\vec{U}\cdot\nabla_H\phi - \overline{w}\, d\phi/dZ - dF_\phi/dZ \qquad (5)$$

allows us, in principal, to predict the evolution of a conservative quantity from an initial measurement. Note that most of the terms in Equation 5 are time and height dependent.

The next step in applying Equation 5 is to consider the boundary layer and free atmosphere separately (in the spirit of Equation 1). In the boundary layer, we integrate Equation 5 to form a layer average (thus the terminology "integrated" model), $\langle X\rangle = 1/h \int_o^h X(Z)dZ$,

$$1/h \int_o^h d\phi_m/dt\, dZ = -1/h \int_o^h [U\cdot\nabla_H\phi + dF_\phi/dZ]dZ \qquad (6)$$

where $d\phi/dZ = 0$ and $\phi = \phi_m$ for $Z<h$. Therefore,

$$d\phi_m/dt = (F_{\phi o} - F_{\phi h})/h - 1/h \int_o^h \bar{\vec{U}} \cdot \nabla_H \phi \, dZ \qquad (7)$$

where $F_{\phi o}$ is the surface flux and $F_{\phi h}$ is the flux at the inversion.

The interaction of the boundary layer with the surface causes ϕ_m to approach the characteristics of the sea surface (via the surface flux, $F_{\phi o}$). Similarly, the boundary layer interacts with the free atmosphere at its upper boundary through a process called "entrainment" (via the flux $F_{\phi h}$). Entrainment is the process whereby free atmospheric air is brought into the boundary layer by the turbulent erosion of the transition region. Thus, entrainment tends to increase h at a rate characterized by the entrainment velocity, W_e, and causes the boundary layer to approach the properties of the free atmosphere. The increase in h is expressed by

$$dh/dt = W_e + \bar{W} - \vec{\bar{U}} \cdot \nabla_H h \qquad (8)$$

Entrainment produces the flux at the top of the boundary layer. This flux is analagous to the surface flux at the sea-air boundary (only in this case the "surface" is the transition zone to the free atmosphere). The entrainment velocity is simply related to $F\phi_h$ by

$$F_{\phi h} = -W_e \Delta\phi \qquad (9)$$

The rate equations for conservative quantities can now be written for both atmospheric regions

$$d\phi_m/dt = (F_{\phi o} + w_e\Delta\phi)/h - \langle\vec{U}\cdot\nabla_H\phi\rangle \quad ; \quad Z<h \tag{10a}$$

$$d\phi/dt = -\vec{U}\cdot\nabla_H\phi - \overline{w}\,\Gamma_\phi \quad ; \quad Z>h \tag{10b}$$

$$d(\Delta\phi)/dt = d\phi/dt)_{Z=h+} - d\phi_m/dt - \Gamma_\phi dh/dt \quad ; \quad Z=h \tag{10c}$$

These equations describe only the evolution due to turbulent transport and large scale advection. For atmospheric quantities of interest (for example, temperature), other processes can appear as source and sink terms. In the case of water vapor, vapor can be lost due to formation of liquid water droplets (condensation) and subsequent loss from rainout. For temperature, there is adiabatic cooling with increasing altitude, latent heat released due to condensation and heat transfers associated with absorption and emission of electromagnetic radiation. Such effects are most easily accounted for by creating an appropriate variable which is conserved. For example, rather than apply Equation 10 to the water vapor mixing ratio, q_v, we use the total water $q_t = q_v + q_\ell$, where q_ℓ is the liquid water mixing ratio. For temperature, we define the moist static energy, H,

$$H = c_p(T + .0098Z) + L_e q_t \tag{11}$$

where c_p is the heat capacity of air and L_e is the latent heat

of vaporization of liquid water. The modifications required to account for radiative flux divergence are now quite simple; rather than use $F_H(Z)$ in Equation 10a, we use the sum of $F_H(Z)$ and the net radiative flux $R(Z)$.

$$dH_m/dt = (F_{Ho} + R_o + W_e\Delta H - R_H)/h - \langle\vec{U}\cdot\nabla_H H\rangle \qquad (12)$$

The application of the total model now requires several steps: 1) parameterization of physical processes (for example, entrainment), 2) development of techniques to obtain the relevant physical data (for example, subsidence velocity $\overline{W}$ and the horizontal gradient terms), 3) development of the relationships of conserved quantities to more meaningful meteorological data (for example, the relationship of temperature to moist static energy), and 4) development of methods to calculate operational variables (for example, profiles of refractive-index structure function parameter, C_n^2) from model variables.

III. MODEL PERSPECTIVE

Before a detailed analysis of the integrated model, it is important to clearly state why this approach cannot be a cure-all for all atmospheric predictive problems. This model contains certain simplifying assumptions that automatically reduce its generality and limit the scope of its application. Requirements for the two layer model are:

1) Clearly defined mixed layer (or at least a capping inversion).
2) Surface evaporation leading to stratus type clouds confined to $h_c < Z < h$ where h_c is the lifting condensation level.
3) Primary source of vertical transport is turbulent mixing.
4) Moderate or predictable synoptic scale thermal changes (a few °C/day).
5) Near adiabatic liquid water profiles in the stratus cloud.
6) Moderate clear-sky net radiative heating changes ($\pm$1°C/day).
7) Moderate or predictable horizontal wind divergence ($|D| \sim 10^{-5}$ sec^{-1}).

Although these assumptions are quite reasonable over a considerable fraction of the world's oceans, there are significant global areas where they break down. For example, in tropical regions much of the vertical transport is due to large scale convergence (the Intertropic Convergence Zone). Because the total water vapor content of the air is greater (higher sea surface

temperatures) the clouds have much more buoyancy from latent heat of condensation. These highly buoyant clouds cannot be confined by the inversion so they break through and rise to great altitudes as classic free convection cells. The large bouyant and turbulent mixing processes in the cloud tend to destroy the adiabatic (equilibrium) liquid water profile. Rather than entraining upper layer air into the mixed layer, the convective cells draw air out of the mixed layer into the cell (and, therefore, the upper air) causing a lowering of the mixed layer height. This process is called cloud induced subsidence or detrainment. Considerable work is now underway to apply the integrated model to this case using an additional layer (two inversions) and parameterizations of cumulus clouds.

Another case for which this model cannot be used is near frontal zones. Clearly, almost every assumption listed can be expected to fail in the vicinity of a strong front. As a result, we do not expect the model to be very useful at higher latitudes during the winter.

Despite these disclaimers, the model does have a wide range of utility. A recent paper by Kraus and Schaller shows examples of mixed layer model application to four different climate regions: tradewind, California coast, Norwegian Sea and the Arctic Ocean (summer).

IV. PHYSICAL PROCESSES

Parameterization of the physical processes is essentially the art of calculating the unknown from the known. For mixed layer models, the known is primarily the mean meteorological profiles, basic atmospheric thermodynamics and a compendium of relevant atmospheric data (such as the radiant intensity from the sun at the top of the atmosphere). This section will be devoted to an examination of various parameterizations used to obtain each term in the rate equations.

A. Surface Fluxes

The bulk aerodynamic method is used to obtain the surface fluxes of momentum, sensible heat and water vapor. The basic assumption of this method is that the flux is driven by the sea-air bulk difference of the variable

$$F_{\phi o} = C_{\phi}^{1/2} (\phi_s - \phi_m) U_* \tag{13}$$

where the subscript "s" refers to the sea-surface value and U_* is the friction velocity

$$U_* = (F_{uo}/\rho)^{1/2} = C_u^{1/2} U \tag{14}$$

where U is the wind speed near the surface ($Z \sim 10m$). The quantity C_ϕ is known as the drag coefficient (typically $C_\phi^{1/2} = 0.035$). The bulk method has been so well verified that it is non-controversial and further discussion in the mixed layer model context is not needed.

B. Clouds

There are several factors to consider when dealing with boundary layer clouds: cloud thickness, liquid water profile and cloud droplet size distribution.

1) The most common assumption is that the cloud bottom is at a height h_c equal to the lifting condensation level. Since we are assuming constant potential temperature (θ=T + .0098Z) and water vapor mixing ratio ($q_v = q_t$) in the noncloud region ($Z<h_c$), h_c is easily calculated from the near surface temperature (T) and dew-point temperature (Td)

$$h_c = (T - Td)/0.00804 \qquad (15)$$

where 0.00804 is the difference in the lapse rate of T and Td under well mixed conditions. However, because h_c is very sensitive to the θ and q profile in the mixed layer, small deviations from the well-mixed assumption (which for most other purposes are not significant) cause large changes in h_c (and, therefore, the cloud radiative effects). Since warm, dry air is entrained into the boundary layer at the top, it is generally observed that q_{tm} decreases and θ_m increases slightly with increasing height in the mixed layer. Therefore, h_c is actually considerably greater (thinner cloud) than h_c calculated from near surface observations using Equation 15. The error can often be more than 100m, which is significant for clouds that are typically 200 to 500m thick. At the moment, only "ad hoc" methods are available for correcting for this effect. These methods allow

q_{tm} and H_m to have small gradients that depend on the surface flux and the entrainment rate.

2) Most mixed layer models calculate the liquid water profile in the cloud based on the same adiabatic assumption (q_{tm} and H_m are height independent for $Z<h$). In other words, given q_t, H and Z one can uniquely determine q_ℓ. Experimentally, it has been found that the liquid water profile is almost always less than the adiabatic value for the reasons explained in part 1. If we use a model that allows a slight decrease of q_{tm} and a slight increase of H_m, then the cloud liquid water profile will be decreased. Since the model contains arbitrary constants, we simply make adjustments to obtain agreement with the measurements (roughly a 30% reduction of liquid water from the adiabatic value).

3) Cloud droplet spectra used in most mixed layer models are based on strictly empirical parameterizations of field measurements. Unfortunately, the measurements are extremely sparse and not very consistent. The most credible data indicates a fairly constant total number density, N, with the mean radius of the cloud drops increasing with height in the cloud ($r_m \sim 2\mu m$ to $r_m \sim 15\mu m$). Sample data are shown in Fig. 3. There are data that indicate fairly constant r_m but an increasing N with altitude (for example, 100 cm^{-3} to 300 cm^{-3}). There is considerable evidence that near the cloud top, variations in liquid water are due to variations in N while r_m remains fairly constant. It has been suggested that this is due to the inhomogeneous mixing of cloud air with newly entrained clear air.

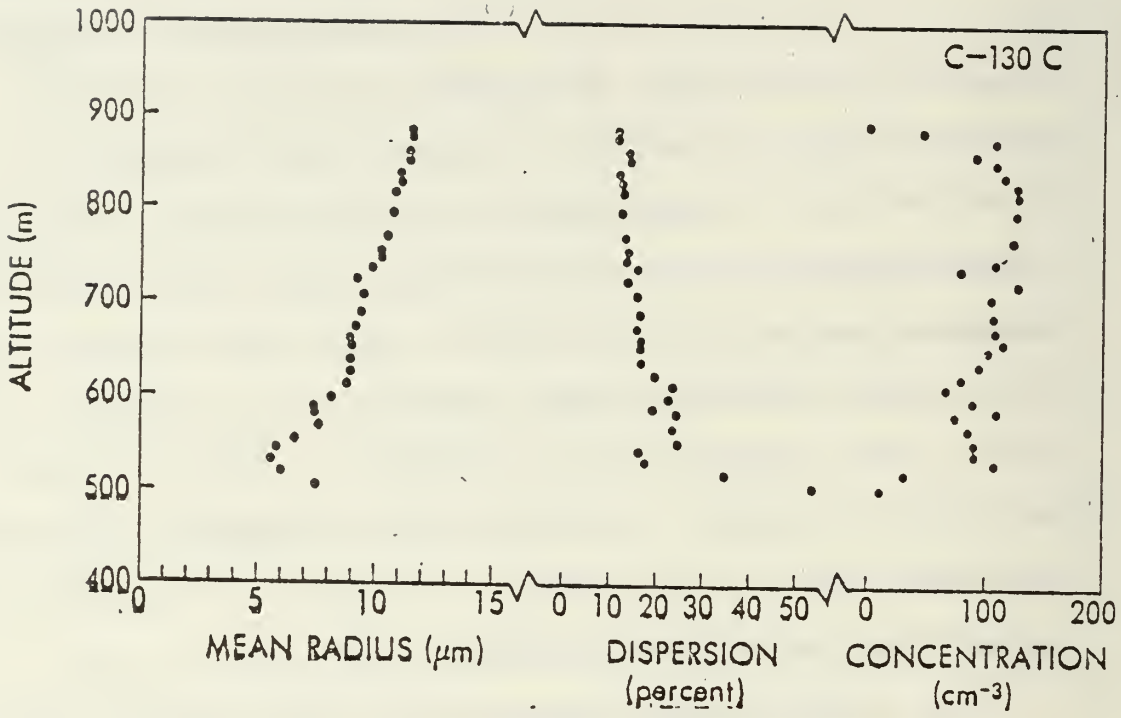

Figure 3. Cloud droplet spectral parameters from mid-Atlantic stratus (Ref.13). The dispersion is the ratio of the standard deviation to the mean radius of the size spectrum.

Obviously, the integrated cloud droplet volume spectrum should give the correct liquid water at each altitude

$$q_\ell \rho = Q(Z) = \rho_w \int_0^\infty 4/3\ \pi r^3 (dN/dr) dr \qquad (16)$$

where ρ_w is the density of water, r the droplet radius and dN/dr the droplet size spectrum. There is also a scale problem because most of the liquid water is in the larger drops ($r>10\mu m$) while most of the shortwave (solar) radiation interaction is determined by smaller droplets. Therefore, one can have two different empirical droplet distributions, both scaled by the liquid water, with quite different short wave radiation absorption. In fact, it has been shown that the longwave emission, short wave absorption and the entrainment rate are all dependent upon the droplet distribution. Since this is a field of very active research, it is probable that good empirical models will be available very soon.

C. Radiation

Mathematical modeling of radiative flux transfer is an extensively developed subject. In general, the radiative effects can be calculated to a precision far exceeding the quality of the input data. In fact, the main problem is to choose a method of minimum complexity appropriate to the accuracy of the data to be used. Unfortunately, even the simple radiative transfer models are still extremely complex in comparison to most other physical parameterizations used in the mixed layer model. Uncertainty in background aerosols, atmospheric absorbing gases (water vapor,

carbon dioxide, ozone) and cloud droplet size spectra are obvious sources of error in radiation calculations. A comparison of two models with aircraft measurements of the radiative flux divergence is shown in Fig. 4.

Most models consider longwave and shortwave radiation separately. Typically, radiation effects are calculated only inside the cloud layer ($h_c < Z < h$). Radiative heating and cooling rates in clear air are on the order of 1°C/day which is approximately the accuracy of even the best models, given typical input data. Earlier models that simply assign a constant long wave cooling rate to the cloud are now considered to be too crude because they neglect the dependence of the downward flux (effective sky temperature) on upper atmosphere properties (primarily water vapor content) and they assume the cloud is totally "black" regardless of cloud thickness. Actually, the emissivity, E, of clouds in the long wave region does not approach unity until $h-h_c \sim 100m$. In the longwave region, the absorption is not extremely sensitive to variations in the droplet spectra typically found in clouds; it turns out that the emissivity can be parameterized in terms of the total liquid water, W

$$W = \int_{h_c}^{h} \rho q_\ell dZ \tag{17a}$$

$$E = 1 - \exp(-0.138W) \tag{17b}$$

Obviously, the integrated cloud droplet volume spectrum should give the correct liquid water at each altitude

$$q_\ell \rho = Q(Z) = \rho_w \int_0^\infty 4/3\ \pi r^3 (dN/dr) dr \qquad (16)$$

where ρ_w is the density of water, r the droplet radius and dN/dr the droplet size spectrum. There is also a scale problem because most of the liquid water is in the larger drops ($r>10\mu m$) while most of the shortwave (solar) radiation interaction is determined by smaller droplets. Therefore, one can have two different empirical droplet distributions, both scaled by the liquid water, with quite different short wave radiation absorption. In fact, it has been shown that the longwave emission, short wave absorption and the entrainment rate are all dependent upon the droplet distribution. Since this is a field of very active research, it is probable that good empirical models will be available very soon.

C. Radiation

Mathematical modeling of radiative flux transfer is an extensively developed subject. In general, the radiative effects can be calculated to a precision far exceeding the quality of the input data. In fact, the main problem is to choose a method of minimum complexity appropriate to the accuracy of the data to be used. Unfortunately, even the simple radiative transfer models are still extremely complex in comparison to most other physical parameterizations used in the mixed layer model. Uncertainty in background aerosols, atmospheric absorbing gases (water vapor,

carbon dioxide, ozone) and cloud droplet size spectra are obvious sources of error in radiation calculations. A comparison of two models with aircraft measurements of the radiative flux divergence is shown in Fig. 4.

Most models consider longwave and shortwave radiation separately. Typically, radiation effects are calculated only inside the cloud layer ($h_c < Z < h$). Radiative heating and cooling rates in clear air are on the order of 1°C/day which is approximately the accuracy of even the best models, given typical input data. Earlier models that simply assign a constant long wave cooling rate to the cloud are now considered to be too crude because they neglect the dependence of the downward flux (effective sky temperature) on upper atmosphere properties (primarily water vapor content) and they assume the cloud is totally "black" regardless of cloud thickness. Actually, the emissivity, E, of clouds in the long wave region does not approach unity until $h-h_c \sim 100m$. In the longwave region, the absorption is not extremely sensitive to variations in the droplet spectra typically found in clouds; it turns out that the emissivity can be parameterized in terms of the total liquid water, W

$$W = \int_{h_c}^{h} \rho q_\ell dZ \qquad (17a)$$

$$E = 1 - \exp(-0.138W) \qquad (17b)$$

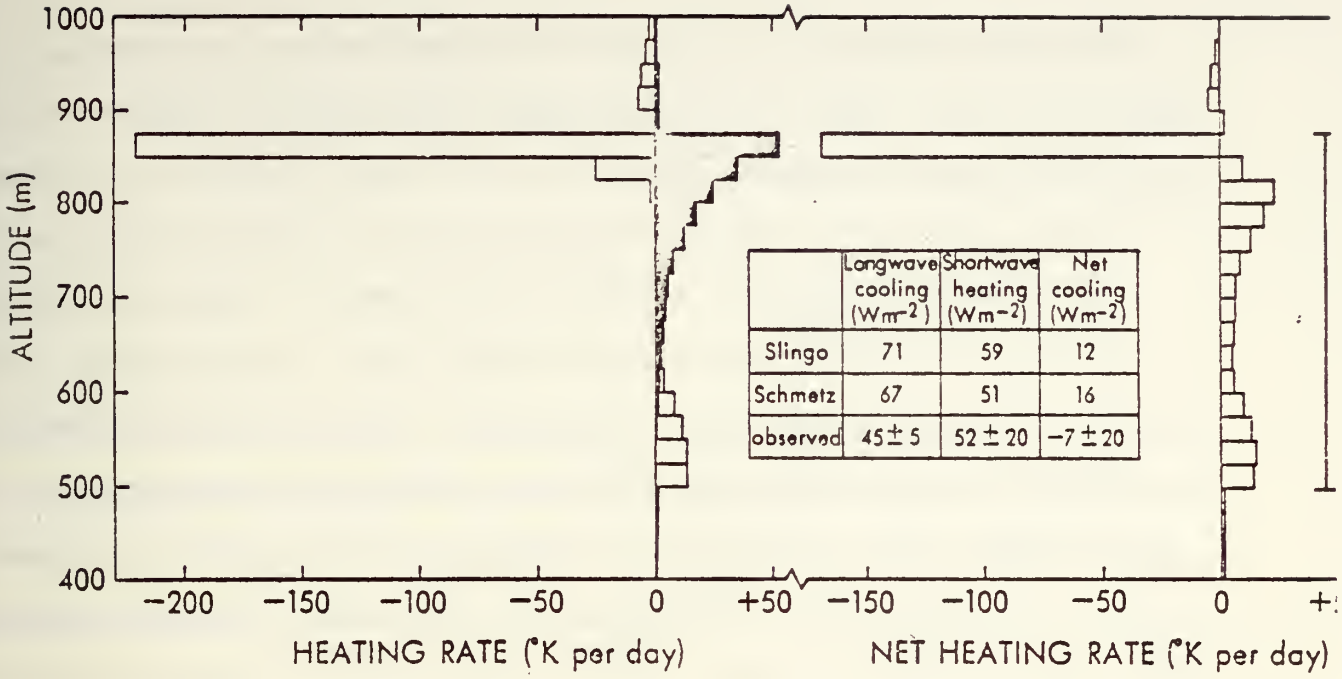

Figure 4. Net shortwave (darkened boxes) and longwave (clean boxes) heating rates (flux divergences) measured from an aircraft are shown on the left. The right side depicts the total radiation heating rate profile. The insert compares these measurements with two recent models (Ref.13).

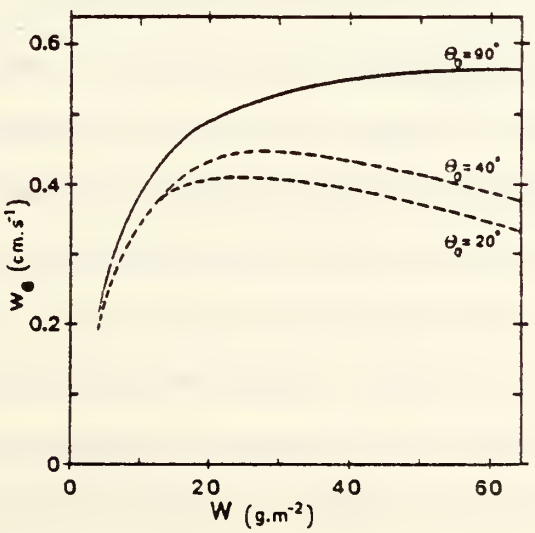

Figure 5. The entrainment rate, W_e, as a function of total integrated cloud liquid water content, W (Eq. 16a). The influence of solar radiation is shown for three different solar zenith angles (Ref. 7). Note $\theta = 90°$ correspond to zero solar flux.

The cloud top cooling rate can be estimated from the cloud top temperature, T_h, and the effective sky temperature, T_{sky}, using the Stefan-Bolzmann law

$$\Delta R_h = E\sigma(T_h^4 - T_{sky}^4)$$

where σ is Stefan's constant. Similarly, the cloud bottom is heated by infrared radiation from the sea surface (which is usually warmer than the cloud). Although this approach is quite simple for calculating the cooling rate, it leads to complications when calculating the effect the radiative flux divergence has on the entrainment rate (which is sensitive to the actual vertical distribution of flux divergence within the cloud). This will be discussed further in the section on entrainment rate.

In the shortwave region, the emissivity approach (Equation 16) is not very useful because shortwave extinction is dominated by scattering (as opposed to absorption). Thus, the direct solar component incident at the cloud top is attenuated rapidly as the cloud is penetrated, but the vast majority of the radiation lost from the direct beam does not warm the cloud, but is simply scattered. This scattered radiation forms a second component usually referred to as the "diffuse" solar radiation. A small fraction of the direct and diffuse radiation is absorbed by the cloud droplets, thus warming the boundary layer. The amount of heating depends on the solar zenith angle, the droplet spectrum, the droplet index of refraction and the albedo of the sea surface.

A number of methods are available for calculating the short wave heating in clouds. The so-called "two stream" approximation, where the scattered radiation is divided into a forward component and a component with an angular distribution calculated from the droplet spectrum, is certainly accurate enough for mixed layer model applications. This method divides the cloud into several (typically four) layers in the vertical to properly account for the redistribution of direct and diffuse radiation as a function of height in the cloud. An excellent review of this subject has been published by Zdunkowski et al (1980).

D. Entrainment

Fluxes at the top of the boundary layer are due to the entrainment of free atmospheric air. We must determine this flux for each variable of interest; for N variables we have N unknown fluxes, $F_{\phi h}$. Eq. 9 relates $F_{\phi h}$ to the entrainment velocity, W_e, and the jump in ϕ across the inversion, $\Delta\phi$. It appears we have traded one unknown ($F_{\phi h}$) for two (W_e and $\Delta\phi$). Actually, one value of W_e is appropriate for all $F_{\phi h}$ and the jumps are not unknowns which must be parameterized but instead are properties which can be modeled from the initial measurements. Thus, we have reduced the N unknown fluxes to one unknown parameter, W_e. The problem left is to determine W_e.

The entrainment process has been investigated through laboratory simulations, three-dimensional numerical models, field measurements (primarily with aircraft) and theoretical simplification of the turbulent kinetic energy balance expressions (this is the

so-called "closure" assumption). The number of entrainment relations available is approxiamtely equal to the number of investigators in the field, which is an indication of the complexity of the problem. Basically, since entrainment is the erosion of the inversion layer by boundary layer turbulence, the entrainment rate depends on the intensity of turbulence at the to of the boundary layer, the stability of the inversion layer and the stability of the upper atmosphere. The virtual potential temperature, θ_v, is an index of the hydrostatic stability of air. If one parcel of air has greater θ_v than another, it is said to be more buoyant. Thus, the jump in θ_v across the inversion, $\Delta\theta_v$, is a primary indicator of the resistance of the inversion to turbulence. Turbulence at the inversion available for entrainment must be either produced at the inversion or transported to the inversion from production regions in the lower parts of the boundary layer. Thus, all processes that create turbulence in the boundary layer are potential sources of entrainment energy. Since turbulence is rapidly dissipated by viscous forces, sources near the inversion tend to be more efficient at enhancing the entrainment process.

The simplest case to deal with is the cloud free boundary layer with negligible jump in the mean wind vector at the inversion. Since the boundary layer turbulence in this case is driven by the surface flux only, the entrainment flux is assumed to be a fraction of the surface flux

$$F_{\theta_v} h = -w_e \Delta\theta_v = -A\, F_{\theta_v} o \qquad (18)$$

where the fraction, A, has been found to be about 0.2. Since $\Delta\theta_v$ must be positive (otherwise, no inversion exists), the negative value of $F_{\theta_v h}$ is simply a reflection of the fact that the boundary layer turbulence must do work to entrain free atmospheric air across the highly stable inversion. Thus, the buoyancy entrainment flux represents a turbulence energy loss mechanism which (along with viscous dissipation) is balanced by turbulence produced in the lower boundary layer that has been transported to the inversion.

Although Eq. 18 is elegant in its simplicity, it is only applicable in cloud free, light wind situations. Clouds are important because they are a source of longwave cooling at the top of the boundary layer. Since cooling at the top is equivalent to heating at the bottom, clouds are source of convective (buoyant) production of turbulence and, therefore, entrainment. Since the longwave and shortwave fluxes are distributed differently in the cloud, the entrainment rate also depends on the shortwave profile (Fig. 5). Assuming one can calculate the cloud properties and and radiative flux profiles, then, in principle, the cloud entrainment contribution can be determined. Some controversy still exists on the correct manner to relate the vertical structure to the horizontal averaging method. The horizontal averaging process enters the problem because of the "bumpy" nature of the top of the boundary layer. It is not known what fraction of cloud top radiative cooling is confined to the mixed layer. This is presently an active research area.

The inversion wind shear, which occurs if there is a jump in the mean wind velocity ($\Delta\vec{U}$), has not received much attention. The importance of wind shear for a given situation can be estimated by the following expression

$$W_e = W_{eo}/(1-R_i^{-1}) \tag{19}$$

where W_{eo} is the entrainment rate due to bouyancy effects and R_i is the inversion Richardson number

$$R_i = g\alpha h\ \Delta\theta_v/(T|\Delta\vec{U}\,|^2) \tag{20}$$

where g is the gravitational acceleration and αh is the thickness of the entrainment region. If $R_i >> 1$, then one can neglect inversion wind shear effects. If R_i is on the order of one, then it is likely that conventional entrainment parameterizations will not be adequate.

V. Synoptic Scale Forcing

The role of synoptic scale air motion on fixed point evolutions was expressed in Eq. 5. For example, typical atmospheric horizontal temperature gradients are on the order of 1°C for 100km. At $|\vec{U}| = 10$ m/s, this could result in an advection temperature change as large as 3.6°C in 12 hours. From the model application point of view, one regards $\vec{U}$ and $d\phi/dZ$ as part of the model initialization and rate equation structure (Eq. 1 and Eq. 10), just as the $\Delta\phi$ data were regarded in the entrainment section. The quantities $\overline{W}$ and $\nabla_H\phi$ are not predicted by the model but are parameters that must be specified in order to make valid predictions. There are three methods that are potential sources of this information: 1) synoptic scale numerical models, 2) multiple station gradient measurements and 3) single station techniques.

The mean vertical velocity, (subsidence) and the horizontal wind gradients (divergence) are phrases that tend to be used interchangeably because they are directly related through mass conservation

$$\nabla \cdot (\vec{U} + \overline{W}\hat{k}) = \nabla_H \cdot \vec{U} + d\overline{W}/dZ = D + d\overline{W}/dZ = 0 \qquad (21)$$

Therefore, the mean vertical motion at height Z is simply

$$\overline{W}(Z) = -\int_0^Z \nabla_H \cdot \vec{U}\, dZ \qquad (22)$$

Often the divergence is assumed to be independent of height below 5km giving

$$\overline{W} = -DZ \qquad (23)$$

A. Synoptic Scale Numerical Models

Synoptic scale methods can be used to calculate $\overline{W}$. The global pressure, temperature and geopotential fields theoretically contain the information required to calcualte the horizontal wind field, $\vec{U}$, the subsidence, and the horizontal gradients of $\vec{U}$ and T. Subsidence can be obtained from direct divergence calculation, several different vorticity methods and thermodynamic methods. At the moment, the global field estimates over the ocean are based so heavily on data obtained over land that these methods are considered unreliable for subsidence and gradient calculations. When over ocean data become routinely available with reasonable density and vertical resolution, synoptic methods will be valuable for the wind field, subsidence and temperature advection terms above the boundary layer. There are presently no plans to develop this resource for water vapor and aerosol advection.

B. Mesoscale gradients

Suppose we wish to consider the evolution of the boundary layer over a 12 hour period. For a typical wind speed (10 m/s), we are concerned with an area roughly 400km on a side. This is really a more mesoscale area of interest. If we have available a network of atmospheric measurements of all relevant phenomena from the surface to several km altitude, distributed over the area of interest, then the horizontal and vertical gradients and the subsidence can be calculated. The classic method of obtaining the divergence is to integrate the horizontal wind field components perpendicular (U_p) to a closed horizontal path

$$\nabla_H \cdot \vec{U} = (1/A) \oint U_p d\ell \qquad (24)$$

where A is the area enclosed by the horizontal path. A minimum of three separate locations (a triangle) is required.

A more general method, which can be applied to a horizontal field of measurements of any variable, is to perform a linear regression on all data points with horizontal coordinates X and Y as variables and slope parameters ϕ_x and ϕ_y, Z held constant

$$\phi(x,y) = a + \phi_x X + \phi_y Y \tag{25}$$

Since $d\phi/dx = \phi_x$ and $d\phi/dy = \phi_y$, then

$$\vec{U} \cdot \nabla_H \phi = U_x \phi_x + U_y \phi_y \tag{26}$$

describes the horizontal advection of the quantity ϕ.

If sufficient data are available (admittedly a big "if"), the mesoscale field method appears to be ideal. However, in addition to the great difficulty involved in operating a marine data network, measurement inaccuracies and atmospheric variability impose inherent limits on the accuracy of this method. For example, a 2 m/s inaccuracy in wind speed (typical for conventional rawindsondes) over a 200km triangle represents an uncertainty in divergence of $\pm$ 1 x 10^{-5} s^{-1}. This could cause an uncertainty in the height of the boundary layer of approximately a factor of two within 24 hours. The problem of atmospheric variability can be solved by averaging a number of near simultaneous (within one hour) atmospheric profiles at each location. For a one minute average, typical wind velocity variability is about 15% of the mean with larger variability at low wind speeds. Thus, wind velocity uncertainty due to variability is, again, on the order of 2 m/s at typical mean wind speed for a single sounding. It appears that the mesoscale mean

field gradient methods must await the deployment of a more accurate, greater horizontal density ocean measurement system.

C. Single Station Analysis

Since local single station data will almost certainly be required for the model initialization, a method that allows estimation of the synoptic terms from these data is ideal. In the case of subsidence, the existing methods require examination of successive radiosonde profiles. One obvious method (basically a "bootstrap" method) is to simply adjust the value of $\bar{w}$ used in the previous time period to obtain agreement of the model. This assumes that the model entrainment rates and boundary layer height advective terms are correct and the only remaining source of error in the prediction of h is the subsidence velocity. One must also assume that the average subsidence over the previous time period is applicable to the current time period.

A second technique utilizes the heating of the upper atmosphere (Z>h) under subsidence conditions. At a given height, the change of potential temperature, d_θ, over the time interval, dt, is related to the subsidence velocity by (Eq. 10b)

$$W = (\vec{U} \cdot \nabla_H \theta - d\theta/dt)/\Gamma_\theta \tag{27}$$

If advection is neglible and the divergence is independent of height, then (using Eq. 23)

$$D = d\theta/(\Gamma_\theta \, dtZ) \tag{28}$$

Note that under these conditions the heating rate is proportional to height, therefore that lapse rate, Γ_θ, will not remain constant in time. Thus, the change in lapse rate with time can be used to estimate divergence

$$D = \ell n(\Gamma_{\theta 1}/\Gamma_{\theta 2})/dt \qquad (29)$$

where $\Gamma_{\theta 1}$ and $\Gamma_{\theta 2}$ are the lapse rates at times t_2 and $t_1 = t_2 - t$.

If accurate estimates of temperature advection are available, subsidence can be accurately obtained using the thermodynamics method (Eq. 27) with a time series of single station temperature profiles. One technique is available to obtain single station temperature advection, the thermal wind method. This method utilizes the known change of the mean wind vector as a function of height due to local gradients of the temperature field. The wind vector change is described by the thermal wind equation

$$\vec{U}_{th} = \vec{U}_1 - \vec{U}_0 = R/f * (\hat{k} \times \nabla\theta)\, \ell n(P_0/P_1) \qquad (30)$$

where 1 and 0 designate different altitudes, P is the pressure, R the gas constant, and $f = 2\Omega \sin(\text{latitude})$ is the coriolis parameter. If we designate

$\nabla_H\theta = d\theta/dx\ \hat{i} + d\theta/dy\ \hat{j}$, then

$$d\theta/dx = +f(V_{1y} - V_{oy})/(R\ \ell n(P_o/P_1)) \qquad (31a)$$

$$d\theta/dy = -f(V_{1x} - V_{ox})/(R\ \ell n(P_o/P_1)) \qquad (31b)$$

If we further designate $\vec{U} = (\vec{U}_1 + \vec{U}_o)/2$, then the advection heating is

$$-\vec{U} \cdot \nabla_H\theta = f(V^2_{1x} + V^2_{oy} - V^2_{1y} - V^2_{ox})/(2R\ell n(P_o/P_1)) \qquad (32)$$

This method does not work in the boundary layer where wind gradients are also caused by the surface stress.

In principle, Eq. 32 and Eq. 27 can be used as single station assessments of W and $-\vec{U} \cdot \nabla_H\theta$. However, since these are <u>difference</u> methods (either between different soundings or different levels within a sounding), they are subject to the same inherent uncertainties due to measurement inaccuracy and normal

atmospheric variability described in the section on the gradient method. Fig. 6 shows a successful comparison of thermal wind and gradient method estimations of temperature advection.

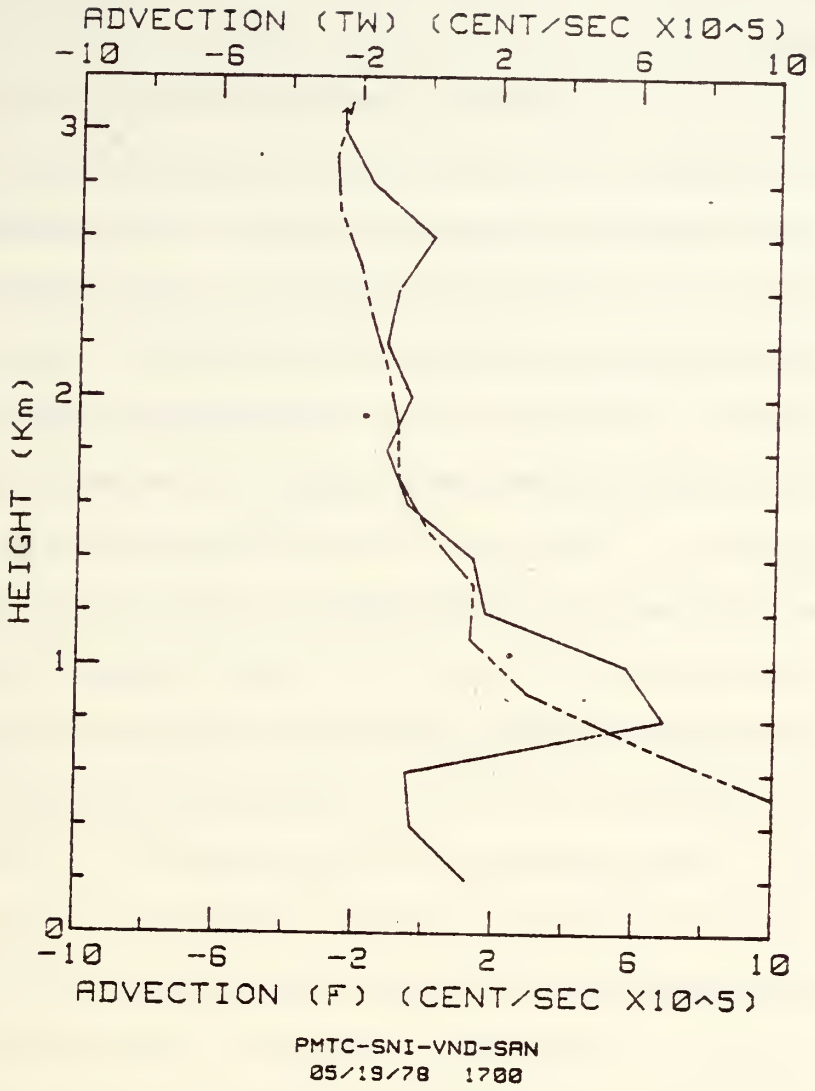

Figure 6. Thermal advection heating rate, $-U \cdot \nabla\theta$, as a function of altitude. The data are obtained from four rawindsonde stations in the southern California coastal region. The solid line is calculated using the thermal wind equation (Eq.32) and the dashed line is from the gradient method (Eq.26). The close agreement of the two methods is not typical.

VI. USER OUTPUT

The basic product of the integrated model is a prediction of the time evolution of the mean profiles (Eq. 4) and the height of the boundary layer. Also available are the various quantities required to drive the model - surface fluxes, cloud thickness, liquid water profiles, long and short wave radiation flux profiles plus external specifications of advective and subsidence effects. This information, which is the direct output of the model, has numerous applications. Certain other relevant data, such as the electromagnetic refractive-index profile, are easily calculated from the model variables (in this case, the temperature and water vapor profiles). There is a third class of information (turbulence properties, for example) which require empirical models for calculation from mixed layer mean profiles.

Typical Navy applications would include basic meteorology, optical propagation, EM (radio and radar) propagation, atmospheric dispersion, remote sensing and oceanographic forcing. In this group, the EM propagation (IREPS), meteorological and oceanographic model structure is very well developed. The optical propagation, atmospheric dispersion and remote sensing applications are not as completely developed (they probably lag the development of the mixed layer evolutionary model at this stage). As an example, the state-of-the-art for optical propagation is discussed in an appended publication. Fig. 7 illustrates how the relevant physical quantity (in this case, the aerosol profile) must be cast in the mixed layer model format to utilize the model predictions.

The following listing summarizes some of the model outputs available either directly (D), through simple calculations (C), or empirical models (M).

1. Meteorology: stratus clouds (D), fog (D), wind-temperature-dewpoint-RH (D), mixed layer height (D).
2. Optical propagation: C_n^2(M), aerosol extinction (M), cloud extinction (M), background radiance (C,M)
3. EM Propagation: M profiles (C), inversion duct strength (C), evaporation duct height (M)
4. Atmospheric dispersion: mixed layer height (D), stability class (C), wind variances (M)
5. Remote sensing: temperature-humidity profiles (D), aerosol profiles (M), clouds (D)
6. Oceanographic: surface fluxes (D), radiation budget - shortwave and longwave (D,M)

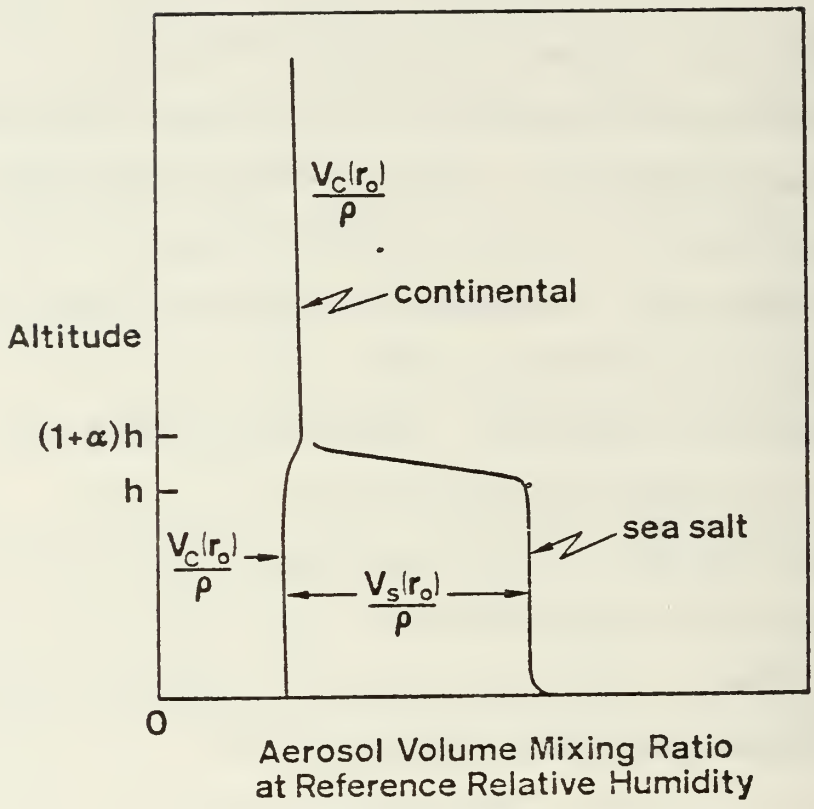

Figure 7. Schematic representation of the atmospheric aerosol distribtuion in the marine regime. The sea salt (locally generated by whitecaps) aerosols (V_s) are confined to the mixed layer while the global backgro continental aerosols (V_c) are present above and belo the inversion.

VII. VERIFICATION

Since we have not outlined a specific integrated type boundary layer model, but have discussed in more general terms the various components available, the question of model verification becomes somewhat nebulous. It is possible to list examples from the literature where specific models have been tested against actual sets of data. Since people rarely publish negative results, these papers generally can be described as "verification" subject to certain caveats about the nature of the agreement. For example, if the divergence is not available, one can find the divergence value that gives the best agreement with the changes of h over the period of interest and then compare the model predictions of the well-mixed θ and q value to the measurements. This is more a test of the self consistency of the model than a test of the model's predictive capability. If the synoptic scale forcing terms are accurate however, the verification is an examination of the integrated mixed layer assumption, and the physical parameterizations used. In view of this, we have arbitrarily designated a set of verification categories that are listed in order from the ideal (1) to the less than ideal.

1) The model was intitialized with data available at the start time and used to make a prediction which was <u>subsequently</u> verified to some stated accuracy in the atmosphere.

2) A complete data set was obtained that allowed an initialization and specification of synoptic scale forcing. The model was found to accurately reproduce the atmospheric measurements.

3) The model was verified on a set of data obtained in laboratory experiments where divergence and advection (presumably) are negligible or known.

4) The model was verified with an adjustable synoptic scale forcing parameter.

5) The model was verified with an adjustable physical parameterization.

A summary of some recently published papers is given in Table I. The results might optimistically be termed "encouraging". Not suprisingly, there is no Type 1 verification. Only one of the Type 2 verifications was made for the marine atmospheric regime and that particular example did not examine the time evolutions but merely verified that the model gave an approximate "steady-state" in agreement with the observations. Obviously a definitive and comprehensive verification of these models has not been done.

Table I. A survey of recently published integrated mixed layer model tests against actual boundary layer evolutions.

Reference	Verification Type	Location	Marine?	Divergence	Advection	Time	Parameters
Stage & Businger 1981	2	Great Lakes	no	measured	Lagrangian	24 hrs.	θ,q,h clouds
Rubenstein 1981	2	East Africa Coast	no	measured	measured	6 hrs.	θ,U,h
Stull 1976	4	Nebraska	no	?	no	12 hrs.	θ,q,h
		Australia	no	?	no	10 hrs.	clouds
		Puerto Rico	yes	?	no	2 1/2 hrs.	
Schaller & Kraus 1981	2	California	yes	measured	measured	steady state	θ,q,h
		N. Atlantic	yes	measured	measured	steady state	clouds
Deadorff 1976	4	Lake Michigan	no	assumed	Lagrangian	13 hrs.	θ,q,h clouds
Deardorff 1979	3	Laboratory	no	----	----	----	θ,h
Davidson, et al 1980	4	California Coast	yes	assumed	no	36 hrs.	θ,q,h

VIII. SAMPLE BIBLIOGRAPHY

Model Mathematical Structures

1. Tennekes, H. and G.M. Driedonks, 1981: "Basic entrainment equations for the atmospheric boundary layer", Boundary-Layer Meteor., 20, 515-531.

2. Deardorff, J.W., 1976: "On the entrainment rate of a stratocumulus-topped mixed layer", Quart. J.R. Met. Soc., 102, 563-582.

3. Deardorff, J.W., 1979: "Prediction of convective mixed-layer entrainment for realistic capping inversion structure", J. Atmos. Sci., 36, 424-436.

Entrainment Relations

4. Stull, R.B., 1976: "The energetics of entrainment across a density interface", J. Atmos. Sci., 33, 1260-1267.

5. Stage, S.A. and J.A. Businger, 1981: "A model for entrainment into a cloud-topped marine boundary layer - Part I. Model description and application to a cold air outbreak episode, Part II. Discussion of model behavior and comparison to other models", J. Atmos. Sci., 37, to appear.

6. Randall, D.A., 1981: "Entrainment into a stratocumulus layer with distributed radiative cooling", J. Atmos. Sci., 37, 148-159.

7. Fravalo, C., Y. Fouquart and R. Rosset, 1981: "The sensitivity of a model of low stratiform clouds to radiation", J. Atmos. Sci., 38, 1049-1062.

8. Schaller, E. and H. Kraus, 1981: "The role of radiation in an inversion capped planetary boundary layer", Boundary-Layer Meteor, 20, 485-513.

Surface Fluxes

9. Garratt, J.R., 1977: "Review of drag coefficients over oceans and continents", Mon. Wea. Rev., 105, 915-929.

10. Friehe, C.A. and K.P. Schmitt, 1976: "Parameterization of air-sea interface fluxes of sensible heat and moisture by bulk aerodynamic formulas", J. Phys. Oceanogr., 6, 801-809.

11. Davidson, K.L., T.M. Houlihan, C.W. Fairall and G.E. Schacher, 1978: "Observation of the temperature structure function parameter over the ocean", Boundary-Layer Meteor., 15, 507-523.

Cloud Structure

12. Slingo, A., R. Brown and C.L. Wrench, 1981: "A field study of nocturnal stratocumulus. Part III. High resolution radiative and microphysical properties", Quart. J.R. Met. Soc., 108, to appear.

13. Slingo, A., S. Nicholls and J. Schmetz, 1982: "Aircraft observations of marine stratocumulus during Jasin", Quart. J.R. Met. Soc., 108, to appear.

Radiation Parameterizations

14. Stephens, G.L., 1978: "Radiation profiles in extended water clouds. Part II. Parameterization schemes", J. Atmos. Sci., 35, 2123-2132.

15. Paltridge, G.W. and C.M.R. Platt, 1976: "Radiative processes in meteorology and climatology". Development in Atmospheric Science, 5, Elsevier, Amsterdam.

16. Roach, W.T. and A. Slingo, 1979: "A high resolution infrared radiative transfer scheme to study the interaction of radiation with clouds", Quart. J.R. Met. Soc., 105, 603-614.

17. Zdunkowski, G.W., R.M. Welch and G. Korb, 1980: "An investigation of the structure of typical two-stream methods for the calculation of solar fluxes and heating rates in clouds.", Contr. Atmos. Phys., 53, 147-166.

Synoptic and Mesoscale Forcing

18. Holton, J.R., 1972: An Introduction to Dynamic Meteorology, Academic, New York.

Miscellaneous

19. Rubenstein, D.N. 1981: "The daytime evolutin of the East African jet", J. Atmos.Sci., 38, 114-128.

20. Fairall, C.W., K.L. Davidson and G.E. Schacher, 1982: "Meteorological models for optical properties in the marine atmospheric boundary layer", Optical Engineering, to be published.

21. Davidson, K.L., G.E. Schacher, C.W. Fairall and T.M. Houlihan, 1980: "Observation of atmospheric mixed-layer changes off the California coast", Proc. Second Conf. on Coastal Meteorology. AMS, Los Angeles, CA.

Figure 1. Block diagram of coupled large scale and boundary layer models for the atmosphere and ocean.

Figure 2. Schematic representation of the two layer model structure for clear sky conserved atmospheric variables-water vapor mixing ratio, Q/ρ, and virtual potential temperature, θ_v. The height of the well-mixed layer is h capped by an inversion of thickness αh.

Figure 3. Cloud droplet spectral parameters from mid-Atlantic stratus (Ref.13). The dispersion is the ratio of the standard deviation to the mean radius of the size spectrum.

Figure 4. Net shortwave (darkened boxes) and longwave (clean boxes) heating rates (flux divergences) measured from an aircraft are shown on the left. The right side depicts the total radiation heating rate profile. The insert compares these measurements with two recent models (Ref.13).

Figure 5. The entrainment rate, W_e, as a function of total integrated cloud liquid water content, W (Eq. 16a). The influence of solar radiation is shown for three different solar zenith angles (Ref. 7). Note $\theta = 90°$ correspond to zero solar flux.

Figure 6. Thermal advection heating rate, $-U \cdot \nabla\theta$, as a function of altitude. The data are obtained from four rawindsonde stations in the southern California coastal region. The solid line is calculated using the thermal wind equation (Eq.32) and the dashed line is from the gradient method (Eq.26). The close agreement of the two methods is not typical.

Figure 7. Schematic representation of the atmospheric aerosol distribtuion in the marine regime. The sea salt (locally generated by whitecaps) aerosols (V_s) are confined to the mixed layer while the global background continental aerosols (V_c) are present above and below the inversion.

Atmospheric Marine Boundary Layer Predictions for Weapons/Systems

Abstract

Weapons/properties of the lower atmosphere are very important in the operation of many systems. Of particular importance is the affect on electromagnetic propagation for the full range from optical to radio wavelengths. Small scale index of refraction fluctuations and aerosols severely affect optical propagation. Large scale changes in the index of refraction cause bending of RF and microwaves, leading to ducting, fading, and a host of other phenomena. Experimental assessment of atmospheric properties can only be done occasionally and on a widely separated basis. Thus, it is critical for operational planning to have available a model which can extend routine atmospheric measurements (radiosonde) in both time and space. At NPS extensive work is underway on modeling the marine atmospheric boundary layer. We sketch here the basics of the model and describe how it can be applied to a wide range of military problems. We illustrate the features being described and the present prediction capabilities.

Contents

1.0 Introduction

Modern warfare has become critically dependent on the entire electromagnetic spectrum for command and control communications, for weapon guidance, for electronic warfare support and for countermeasures. Tactically essential systems are highly affected by the environment even when conditions are not severe in the historical sense. Enhancement or degradation of EM/EO system operational performances has become a primary concern of task force commanders. As such, the deployment of resources and the modification of tactics based on environmental factors in EM/EO propagation will, to a very large extent, determine the effectiveness of sensor, weapon and communication systems.

Environmental effects on EM/EO system performance can be grouped in the general categories of refraction (EM), wave front distortion (EO), extinction (EO), and particulate dispersion (EM/EO). Environmental factors contributing to these effects are the vertical gradients of temperature and humidity for refraction, small scale inhomogeneities (turbulence) of the index of refraction for optical wave front distortion, concentrations of water vapor and aerosols for extinction (absorption and scattering) and turbulent transport for dispersion. All of these factors are multi-variable in terms of the dependence on routinely measured and predicted meteorological variables; pressure, wind, temperature and moisture. The only factors for which accuracies of existing and foreseen measurements approach direct descriptions of the effect is that of gradients of index of refraction and absorption. Turbulence and aerosol descriptions will have to be obtained by indirect methods due to measurement complexities which preclude direct measurement on operational ships.

We are interested in describing all these factors for the atmospheric region extending from the surface to .5 - 2 km above the surface, the marine atmospheric boundary layer (MABL). The MABL is cooler and more moist than the overlying air and is capped by a layer (inversion), 50-100 meters thick, in which temperature increases and humidity decreases with height. Critical values of the index of refraction gradients leading to EM propagation anomalies may exist within the shallow capping inversion because of the humidity and temperature gradients. The entire affected region (duct) extends below the inversion and determining its lower boundary is essential. High turbulence occurs in the inversion as well as in the surface layer and can cause degradation of horizontal and slant path optical propagation. Inversion turbulence intensities are usually 1 to 2 orders of magnitude greater than those below and 2 to 3 orders of magnitude greater than those above. Tactically significant extinction of infrared energy is due to water vapor absorption and marine aerosol scattering in the presence of high humidity and, thus, is usually restricted to the MABL.

All of the above features depend critically on the detailed vertical structure of the atmosphere; so regional climatologies are not useful for operational predictions. This is because the significant vertical structures are lost in averaging, and also because most historical measurements do not relate to specific EM/EO requirements. Furthermore, the strengths of the gradients and their levels, and hence, the affected regions cannot be explained on the basis of large scale atmospheric flows since they are controlled by near surface dynamic processes as well as larger scale features.

We believe a 'gap' has existed in past efforts to characterize tactical environmental conditions. The gap was between two extreme approaches of relating conditions to 1) near surface observations, and 2) to larger scale predicted synoptic patterns. Clearly, to assess the above features, local measurement is desirable. Measurements (radiosondes) are made infrequently and, as time progresses, the initial point measurement becomes less applicable and a predictive scheme is needed. One must consider a transition to climatology, large scale numerical analysis predictions, or dynamic models based on the initial soundings which are available at the operational location. Climatology has already been addressed and discounted. Ruggles (1975) has examined the capabilities of large scale numerical procedures at remote facilities and argued convincingly that they are not sufficient.

Needed are characterizations of coupled local oceanic and atmospheric mixed layer features for time scales from 12 to 18 hours and for spatial scales from 50 to 300 km. Significant changes occur in both mixed layers over these temporal and spatial scales. Predicting these changes is now possible using available measurements and reasonable physical models which have been recently formulated.

This paper will describe results from observational and model evaluation/reformulation efforts which provide evidence that tactically relevant forecasts are possible over the required time and space scales. The MABL will be considered but, as will be seen, the MABL model must eventually be coupled with an Ocean Boundary Layer (OBL) model to adequately describe the changes in both layers.

The long term objective of work in these areas is to make reliable 6-18 hour forecasts of properties within the MABL and OBL. The near term objectives are 1) to verify and reformulate existing models for the responsible physical processes and 2) to develop measurement procedures which are suitable for routine observations from a single ship or aircraft. It will be necessary for the finalized model to predict such properties as the height of the inversion, the strength of the gradients and fluxes at the inversion and at the surface, and the values of well mixed properties in the region between the surface and the inversion.

2.0 Background

This section will provide a general outline of the required descriptions and the models which can be used to predict them. The descriptions and models are delineated in Figure 1, where the descriptions are enclosed by ellipses and models and measurements are enclosed by rectangles. The meteorological descriptions and models are enclosed by a dashed outline. Tactical descriptions (forecasts) to which the improved understandings would apply appear on the extreme right hand side. Single station assessment constraints associated with the local atmospheric and ocean models are timely and compatible with the concept of the Tactical Environmental Support System (TESS) as recently described by NEPRF scientific personnel (NEPRF METRO Report, July 1981).

As stated, we will only consider the local atmospheric mixed layer model and associated descriptions. The local oceanic descriptions would be made by an oceanic mixed-layer model (e.g., Garwood, 1977) and the regional descriptions would be made by a three dimensional atmospheric (e.g. NORAPS) and a regional oceanic (e.g. TOPS) numerical prediction model. The ocean mixed layer model and the regional numerical prediction schemes are objectives of other Navy sponsored basic and exploratory research efforts.

2.1 Meteorological descriptions and models

From a local assessment perspective, let us consider an idealization of the oceanic-atmospheric system. The sea-air interface is bordered by oceanic and atmospheric turbulent mixed layers which effectively insulate the bulk ocean and atmospheric regions. The primary sources of the turbulence within the layers are the velocity (current) and buoyancy (density) gradients at the interface. Even under conditions where the water is slightly cooler than the air, buoyancy forced velocity fluctuations within the layer can be quite large and mix the entire MABL from the surface to the inversion. The large vertical mixing yields constant (well-mixed) wind, temperature and humidity profiles above the surface. At the top of the atmospheric mixed layer there is a thin transition region (inversion). Examples of observed well-mixed profiles and the inversion are shown in Figure 2(a).

The atmospheric mixed layer interacts with the free atmosphere at the inversion by means of turbulence forced entrainment. Entrainment brings dry, warm air into the mixed layer and also increases the surface winds if there are higher winds aloft. Stratus clouds would form within the layer if entrainment caused the moist mixed layer to extend above the condensation level.

Physical processes within the mixed layer are also controlled or forced (over a time scale of 24-36 hours) by the large scale, non-stationary, synoptic flows. Synoptic scale mean vertical motion and advection will have to be prescribed or predicted over the forecast period.

The previously inferred well-mixed nature of the convective MABL has implications for the vertical distributions of mean values and the vertical fluxes (transports) of wind, temperature and humidity. One implication already illustrated is that properties which are conserved during mixing can be treated as being constant with height within the MABL. These parameters are the specific humidity and potential temperature for a clear MABL and equivalent potential temperature and total (vapor plus liquid) specific humidity for a cloudy MABL. A second implication is that vertical fluxes of the well-mixed parameters decrease linearly with height.

These implications enable predictions of MABL evolution to be based solely on fluxes at the upper (inversion) and lower (surface) boundaries and the large scale subsidence and advection. They form the basis of recent model formulations by Deardorff (1976) and Stage and Businger (1981). Fluxes of both boundaries are due to buoyant and mechanical generated turbulence for the clear case with the addition of cloud top radiative fluxes for the cloudy case. The linear height variations of the fluxes allow one to relate buoyant fluxes at the inversion to the more readily estimated surface fluxes. Also, cloud top radiative fluxes can be estimated on the basis of general cloud features. Approaches exist for estimating synoptic scale forcing from single station measurements but further efforts are required to achieve the accuracies required in MABL predictions.

In general, existing models are quite good for the clear sky MABL and fair to good for the cloudy MABL. Considerable effort is now being directed to improving the models for the cloudy MABL. The existence of cloud layers in the MABL is very sensitive to both the sea surface temperature and the entrainment rate and, in turn, clouds have a profound effect on the short and long wave radiation budget at the surface. Fairall et al (1982) provide our position discussion on the approach and the status of abilities to predict the evolution of the MABL.

2.2 Tactical descriptions

Figures 2b-d illustrate tactical descriptions discussed in the Introduction and appearing in the right hand column of Figure 1. Meteorological processes and features relevant to these tactical descriptions are those that were discussed above (Figure 2a and column 4 of Figure 1). Several meteorological factors affect each tactical description as indicated by the numbers, 1-4, in Figure 1. A few of the significant properties and values in the tactical descriptions are described in the following paragraphs.

The M profile in Figure 2b describes the refracted EM ray radius of curvature, relative to the earth's radius of curvature. If M decreases with height, a trapping layer is formed because the EM ray will bend downward relative to the earth. This causes the formation of a duct. The upper boundary of the duct is at the M minimum; the lower boundary is at the height where this same value of M occurs below the trapping layer, as shown in Figure 2b. The M profile is determined by pressure, temperature

and humidity profiles, so values of well mixed temperature and humidity determine the lower boundary of the duct. An increase of mixed layer M value with time could cause an elevated to become a surface based duct as shown in Figure 2b. This could occur if the mixed layer became warmer and drier due to entrainment of overlying air. (Warming and drying of the mixed layer by entrainment would also increase the height of the evaporation duct, a ducting layer immediately adjacent to the surface.) Examples of extended ranges and holes occurring with a duct appear in Figure 3 (Hitney, 1979).

The C_N^2 profile in Figure 2c shows the vertical variation of turbulence which would affect optical wave front distortion. We see that C_N^2 is largest near the surface and in the inversion. Values in these regions are 1-2 orders of magnitude larger than those in the mixed layer and above the inversion. C_N^2 values near 10^{-14} $m^{-2/3}$ are representative for these two regions. The importance of this value is illustrated in Figure 4 with a simulated image of a remotely piloted vehicle as viewed through C_N^2 regions of 0 (no turbulence), 10^{-15}, and 10^{-14} $m^{-2/3}$ (Kearns and Walter, 1978).

The extinction coefficient, β, profile is shown in Figure 2d. β is inversely proportional to the range of IR systems and depends on the absolute humidity and the aerosol size distribution. Aerosol size distributions depend on the generation rate of sea salt particles and on the relative humidity through the growth factor. Therefore, IR extinction is very dependent on the entrainment of relatively clean, dry and warm air from above the inversion and on the surface wind generation of the sea salt particles. As illustrated, the extinction coefficient is large within the mixed layer and increases with height due to relative humidity increases. The increase with height is important in slant path range considerations.

3.0 MABL observations and predictions

A recently obtained data set will be used to demonstrate the nature of changes in the MABL and their prediction. The demonstration will show:

a) the status of available data sets,

b) that the assessment of relative roles of dynamic processes in the MABL can be based on a relatively simple physical model which includes specifiable inputs, and

c) that, at the present time, we have only initial evidence that changes can be predicted. The rigorous specification or description will require further interpretive efforts and, perhaps, improved formulation of the separate models.

3.1 MABL observations

The data were obtained during the Cooperative Experiment on West Coast Oceanography and Meteorology (CEWCOM-78) conducted west of San Nicolas Island, CA during May of 1978. Observations of the oceanic and atmospheric mixed layers were made from the R/V ACANIA; radiosonde observations were also made at surrounding shore stations. The data to be shown are from a 48-hour period, 5/19/1200 to 5/21/1200 PST. The R/V ACANIA was cruising slowly (2-3 knots) into the wind and returned to an initial point approximately every 12 hours. The general location of the R/V ACANIA during the 5/19 to 5/22 periods and locations of surrounding shoreline radiosonde sites appear in Figure 5.

The period was one of steady onshore flow caused by the combined effects of intensification of the Eastern Pacific High and the persistence of the Mexican thermal low. The only apparent change in synoptic scale forcing was an increase in the offshore pressure gradient. Advection in the atmosphere was moderate. However, MABL evolutions were primarily determined by subsidence, surface fluxes, and entrainment at the inversion. Satellite imagery showed increasing uniform stratus coverage (thin to heavy) during the period with a cellular (broken) coverage occurring late on the 21st.

Acoustic sounder returns, mean surface layer parameters, and sea surface temperature during the 19-21 May period are shown in Figures 6b-d, all measured from the R/V ACANIA. Potential temperature composite profiles from shipboard and shore station radiosonde and temperature profiles from ship deployed XBT's appear in Figures 6a and 6e, respectively. Although these descriptions of MABL and CBL changes were obtained from an instrumented research vessel, all can be obtained from operational ships. This includes the acoustic sounder record.

Changes of atmospheric features which would have been tactically significant in view of the time scale and their magnitudes were:

a) The MABL depth increased from 250 m to 750 m over the 48 hour period. The changes occurred in relatively short intervals, from 20/00 to 20/04, and from 21/00 to 21/08. The ABL depth remained near constant during the intervening 12 to 18 hour periods.

b) The surface layer temperature increase from 20/00 to 20/15 is indicative of entrainment of overlying warm air. Entrainment would also dilute the mixed layer and decrease the relative humidity. The entrainment was presumably also a factor in the wind speed increase over the same period, which caused the warm

shallow ocean layer to be destroyed, lowering the sea surface temperature after 20/1800 (Figure 6d).

In conjunction with changes in MABL structures and parameter values depicted in Figure 6, changes occurred which are important to operational systems. Some of these changes can be determined directly from parameters measured in this scientific observational effort. M profile and cloud base heights (condensation levels) can be calculated from the measured humidity and temperature profiles. Surface layer extinction coefficients have to be determined from the measured humidity and aerosol size distributions. Our approach for determining extinction coefficients from aerosol data has been described by Schacher et al (1981). Surface layer C_N^2 values and evaporation duct heights can be determined with considerable certainty from measured surface layer wind, temperature, humidity and surface temperature values using expressions described by Davidson et al (1981) and Fairall et al (1978), respectively. Extinction and C_N^2 profiles have to be based on more recent and, hence, less substantiated expressions such as those by Wells et al (1977) and Wyngaard and Lemone (1980).

Results from these determinations appear in Figures 7 and 8 along with the composite potential temperature, θ, and water vapor mixing ratio, q, profiles (Figure 7a) and the inversion height (Figure 8a, rectangles). The observed results are the solid lines for profiles (Figure 7) and the X's for observed (Figure 8). The observed inversion heights (Figure 8a) (the rectangles) are shown for all stations used in the composites. The observed results indicate that for the observation period:

a) The EM duct associated with the inversion gradients evolved from being surface based to being elevated (Figure 7b) and the evaporation duct height ranged from below 5 m to above 8 m (Figure 8b),

b) Optical turbulence, C_N^2, in the surface layer varied from 10^{-15} to 10^{-14} $m^{-2/3}$ over the period (Figure 8c) and values in the inversion increased from 10^{-16} to 10^{-15} $m^{-2/3}$ (Figure 8c),

c) Surface layer aerosol extinction in the 8-12 μm IR region increased during the first 6 hours (5/19 1200-1800) because the relative humidity increased. It decreased during the last 18 hours (5/20/1800 to 5/21/1200) because of relative humidity and wind decreases (Figure 8d),

d) stratus cloud persisted through the period. The base lifted from about 100 m at 5/19/1800 to 600 meters at 5/21/1200. This is evident in the extinction profile (Figure 7d).

3.2 Model predictions

During the past five years, we performed investigations on surface layer and mixed-layer scaling of small scale turbulence and aerosol properties (Davidson et al, 1978; Fairall et al, 1979; Schacher et al, 1981). The investigations led to the application of a time dependent MABL model based on entrainment energetics and on cloud radiative transfers suggested by Deardorff (1976). The model requires as input an initial atmospheric sounding (radiosonde), the mean winds at a level within the surface layer (10-30 meters) and the surface temperature. Well-mixed temperature and humidity are predicted so the surface wind and wind shear at an inversion are the only local atmospheric variables which have to be prescribed. The larger scale subsidence and advection must also be prescribed for the forecast period.

The steps in the prediction computation are shown in Figure 9, where it is noted that procedures are the same for clear and cloudy cases except for entrainment computation and estimating cloud top cooling. Fairall et al (1982) include comprehensive discussions of how responsible physical processes are treated in the model and how available data can be used to estimate the processes. Because of the simplified physical model the computations do not require numerical integrations on a vertical grid so the computer storage requirements can be satisfied by available shipboard microcomputers. In fact, we are examining the use of a hand-held calculator for the procedures.

Predictions of MABL changes were made with the simplified model for the 48 hour period (5/19/1200 to 5/21/1200) corresponding to observed results in Figures 6a-e. The predictions were made for two separate 24 hour periods starting at 19/1200 and at 20/1200. Initial profiles for the 19/1200 start time was that obtained at San Clemente Island (SCI in Figure 5) at approximately 1000. Initial profiles for the 20/1200 start time were averages of the composites at 20/0500 and 20/1700. The sea surface temperatures were those at each start time as shown in Figure 6d and were 15 and 14.5 C. The surface wind observed during the forecast period was specified to increase linearly from 5 m s^{-1} at 19/1200 to 10 m s^{-1} at 20/2100 and then to decrease linearly to 7 m s^{-1} at 21/1200.

Larger scale synoptic forcing (subsidence and thermal advection), stated previously as requiring more study if it is to be satisfactorily estimated from single station assessments, was estimated from temperature changes above the inversion (subsidence) and from the thermal wind (thermal advection). It was set to zero during the first period. Subsidence for the second period, starting at 20/1200, was adjusted on the basis of that value required for agreement between predicted and observed mixed layer depths during the first period. Hence, the model was also used to estimate the "most probable" synoptic scale subsidence.

The predictions are illustrated in Figures 7 and 8 along with the "observed" results. The predictions are the dashed lines for both the profiles (Figure 7) and inversion height and surface layer, 10 m, values (Figure 8). The agreement near 20/1200 in Figure 8 occurs because the

model was reinitialized at that point. Significant outcomes from comparisons of observed and predicted results are

a) The mixed layer depth (inversion height, Figure 8a) was predicted quite well. This increase during the later part of both periods was caused by cloud top entrainment because the predicted surface layer stability became stable and, hence, there existed no surface buoyancy flux forcing.

b) The cloud cover was accurately predicted to persist throughout the first period and for the first 15 hours of the second period, as indicated by the condensation level being below the inversion in Figure 8a. However, the predicted cloud thickness was less than that which actually occurred. As indicated in preceding discussions, the cloud cover was observed to break up in the 21st and the prediction after 21/0600 agrees with that.

c) The well mixed temperature and humidity and the jump predictions (Figure 7a) are reasonable except for the 20/0500 comparison time. The predicted well mixed temperature was too warm (1-2 C) at all other comparison times. This led to the surface layer becoming stable when in actuality it remained unstable throughout both periods, surface temperature higher than 10 m temperature. We believe the cooling associated with the clouds was not sufficient. It will be seen that the surface layer was stable (too warm) during the night hours.

d) The predicted M profiiles (Figure 7b) were very accurate in terms of the surface based duct evolving to an elevated duct and the lower boundary. It is interesting that even when the predicted well mixed temperature and humidity were much too high (20/0500) the M. profile verified. This occurred because their respective affects on M compensated.

e) The predicted C_N^2 profiles (Figure 7c) gave good values for the inversion region and reasonable values for the mixed layer, except for 20/0500. It is noted that values above the inversion were set to 10^{-18} for both observed and predicted profiles. Factors of 3 agreement are considered reasonable for C_N^2. It is noted that inversion region values should be based on the convective mixing velocity, W_* (Wyngaard and Lemone, 1980). When a stable surface layer existed (20/0500) the friction velocity, U_*, was used instead of W_*.

f) The total extinction at 8-12 μm prediction (Figure 7d) was quite good outside of cloud layers. Again, values above the inversion were set to the same value for both observed and predicted profiles. The sensitivity of aerosol size to relative humidity changes when the relative humidity is above 90% is what leads this comparison to give seemingly poor results. Hence, the good agreement outside of clouds is encouraging.

g) The evaporation duct height (Z_*) prediction (Figure 8b) is not very good. The disagreement occurs because the predicted surface was less unstable (more stable) than the observed. Z_* increases almost linearly with increasing stability. The very large predicted Z_* values at the end of the second period occurred because it was stable and because the predicted well mixed humidity decreased, Figure 7a.

h) The predicted surface layer C_N^2 values (Figure 8c) were always less than those observed because of the previously mentioned inaccurate surface layer stability. The minima at 19/2300, 20/1800 and 20/0500 correspond to the surface layer going from unstable to stable, unstable to stable and stable to unstable, respectively.

i) The predicted surface layer aerosol scattering extinction for 8-12 μm (Figure 8d) was very good during the second period. The observed and predicted decrease from 20/1800 to 21/1200 was associated with due to a decrease in relative humidity and wind speed. The wind speed used for the prediction was, of course, prescribed on the basis of observed results. Hence, the role of relative humidity on the extinction is that being evaluated.

4.0 Conclusions

The importance of and an approach for predicting evolutions of the marine atmospheric boundary layer have been described. Any change in the mixed layer depth or well-mixed properties can lead to significant changes in the weapons/systems tactical environment. These include EM duct regions, optical turbulence and optical extinction, both within and at the boundaries of the inversion capped mixed layer.

Although the tactical descriptions are multi-variable and require detailed vertical descriptions, a simplified model based on routinely observed data appears to be quite useful for predicting changes over 12-18 hours. For the cloud topped period considered, the refraction,

optical turbulence and optical extinction profiles were predicted quite well. Cloud coverge changes were also predicted quite well. The primary differences between observed and prediction results were for the surface layer, the evaporation duct height and the optical turbulence. The differences were significant in terms of tactical effects. The predicted evaporation duct was much too high and the predicted optical turbulence was much too low. The reason in both cases was that the predicted air temperature was too high (2-3 C) which resulted in a neutral to stable condition. We believe the cause for this was the improper specification of cloud cooling within the mixed layer.

5.0 Acknowledgments

Our work has been supported by NAVAIR (AIR-370) in MABL model development, NAVMAT (Navy ECMET) in aerosol measurements and NAVSEA (PMS-405) in optical turbulence. We gratefully acknowledge the assistance of Ms. Patricia Boyle in preparation of the manuscript and Drs. A. Goroch (NEPRF) and B. Katz (NSWC, White Oak) for providing advice and direction in the areas of optical turbulence and extinction.

6.0 References

Davidson, K. L., T. M. Houlihan, C. W. Fairall and G. E. Schacher, 1978: "Observation of the temperature structure function parameter over the ocean", Boundary-Layer Meteor., 15. 507-523.

Davidson, K. L., G. E. Schacher, C. W. Fairall and A. Goroch, 1981: "Verification of the bulk method for calculating overwater optical turbulence", Applied Optics, 20, 2919-2924.

Deardorff, J. W., 1976: "On the entrainment rate of a stratocumulus-topped mixed layer", Quart. J. R. Met. Soc., 102, 563-582.

Fairall, C. W., K. L. Davidson, G. E. Schacher and T. M. Houlihan, 1978: "Evaporation duct height measurements in the mid-Atlantic", Naval Postgraduate School Technical Report NPS-61-78-001, 106 pp.

Fairall, C. W., G. E. Schacher and K. L. Davidson, 1980: "Measurements of the humidity structure function parameters, C_q^2 amd C_{Tq}, over the ocean", Boundary-Layer Meteor., 19, 81-92.

Fairall, C. W., K. L. Davidson and G. E. Schacher, 1981: "A review and evaluation of integrated atmospheric boundary layer models for Maritime applications", Naval Postgraduate School Report NPS-63-81-00X, 39 pp.

Garwood, R. W., Jr., 1977: "An oceanic mixed layer model capable of simulating cyclic states", J. Phys. Oceanogr., 7, 455-468.

Hitney, H. V., 1979: "Integrated refractive effects prediction system (IREPS) and environmental/weapons effects prediction system (E/WEPS)," Proceedings, Conference on Atmospheric Refractive Effects Assessment 23-25 January 1979, Naval Ocean Systems Center Technical Document, NOSC PD 260, 13-17.

Rosenthal, J., T. Battalino, H. Hendon and V. R. Noonkester, 1979: "Marine/continental history of aerosols at San Nicolas Island during CEWCOM-78 and OSP III Pacific Missile Test Center, Point Mugu, Report TP-79-33, 306 pp.

Ruggles, K. W., 1975: "Environmental support for electro optics systems", Fleet Numerical Weather Central Technical Report 75-1, Monterey, CA, 47 pp.

Schacher, G. E., K. L. Davidson, T. M. Houlihan and C. W. Fairall, 1981: "Measurements of the rate of dissipation of turbulent kinetic energy, ε, over the ocean", Boundary Layer Meteor., 20, 321-330.

Schacher, G. E., K. L. Davidson, C. W. Fairall and D. E. Spiel, 1981: "Calculations of optical extinction from aerosol data", Applied Optics, to appear.

Stage, S. A. and J. A. Businger, 1981: "A model for entrainment into a cloud-topped marine boundary layer - Part I. Model description and application to a cold air outbreak episode. Part II. Discussion of model behavior and comparison to other models", J. Atmos. Sci., 37, to appear.

Wells, W. C., G. Gal and M. W. Munn, 1977: "Aerosol distributions in the maritime air and predicted scattering coefficients in the infrared, J. Appl. Opt., 16, 654-659.

Wyngaard, J. C. and M. A. Lemone, 1980: "Behavior of the refractive index structure parameter in the convective boundary layer", J. Atmos. Sci., 37, 1573-1585.

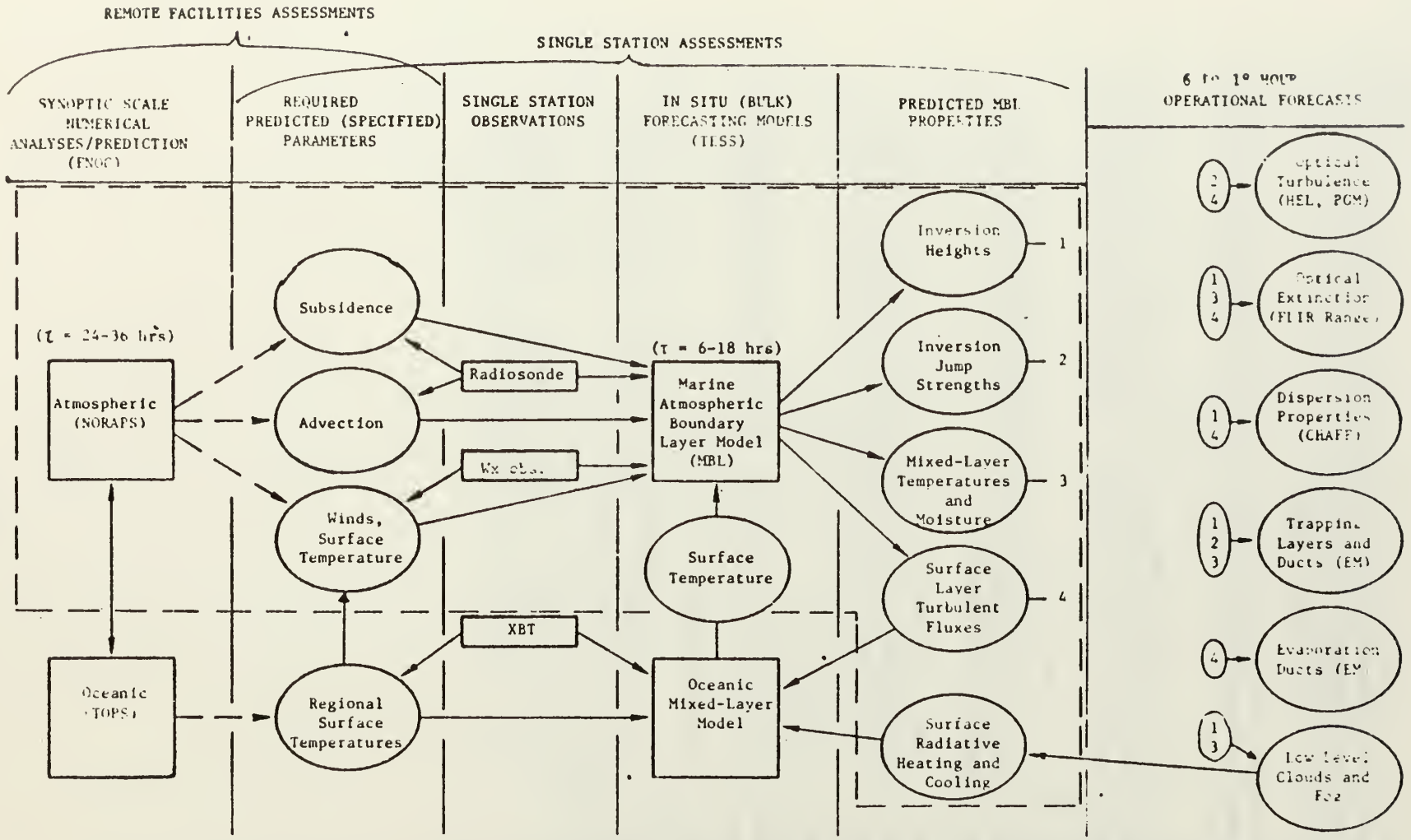

Fig. 1: Illustration of input parameters, predicted properties and operational forecasts associated with a bulk atmospheric boundary-layer model (MABL). Numbers to the left of operational forecast items pertain to the required predicted MABL properties. The bulk atmosphere and ocean mixed-layer models would be coupled in a shipboard, aircraft micro-computer. Dashed lines (- →) coming from remote facilities imply that the required information could be obtained from these but the in situ capabilities should be possible without these sources.

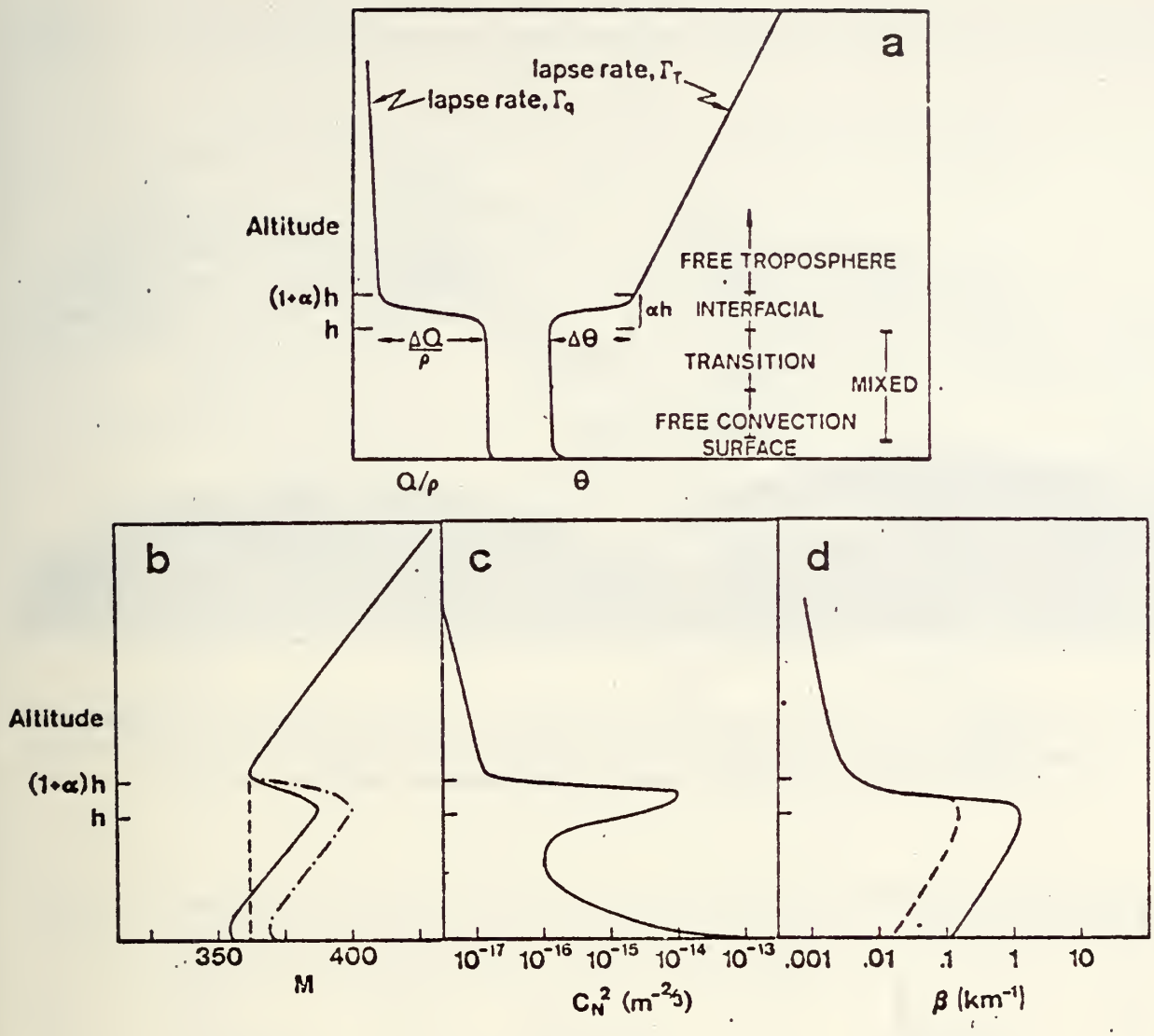

Fig. 2. Simplified meteorological and tactical features of the MABL and overlying region including (a) humidity mixing ratio, Q/ρ, and potential temperature, θ, profiles and subregions, (b) modified index of refraction, M, profiles, (c) optical turbulence intensity, C_N^2, profiles, (d) total extinction coefficient, β (absorption and scattering), profile.

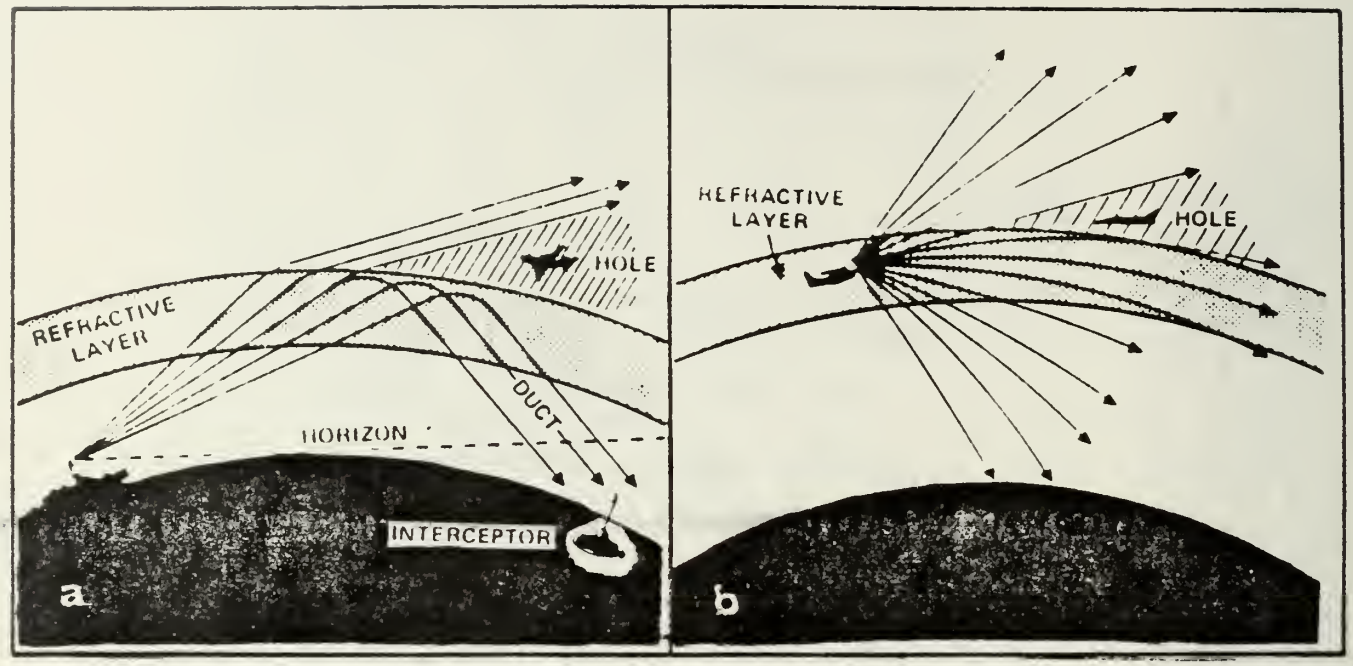

Fig. 3. Examples of extended ranges and holes for EM ducts for (a) surface-based duct and a shipboard air-search radar and (b) elevated duct and an airborne early-warning radar (from Hitney, 1979).

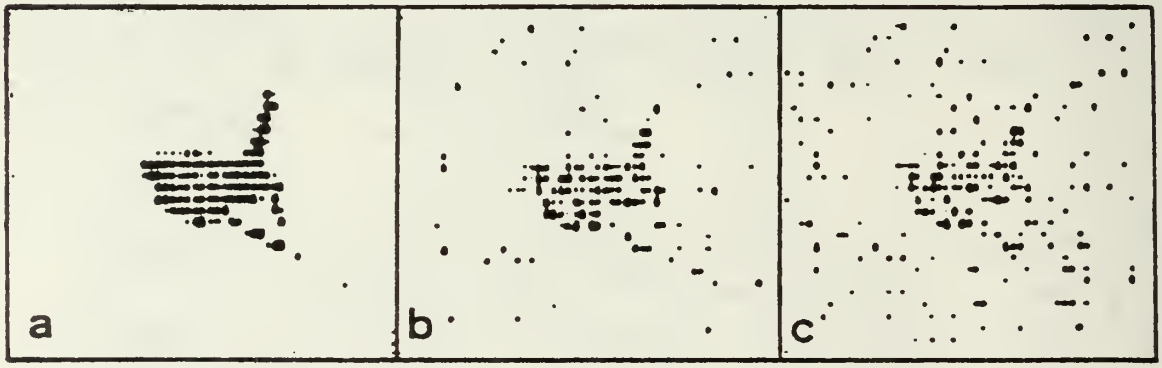

Fig. 4. Computer simulated image remotely piloted vehicle (RPV) as viewed with 8-12 m IR sensor (range 2 km, visibility 15 km, threshold 4.5 nW) through atmosphere with C_N^2 values of (a) 0 (no turbulence), (b) 3.7×10^{-15} $m^{-2/3}$ and (c) 1.0×10^{-14} $m^{-2/3}$ (from Kearns and Walter, 1978).

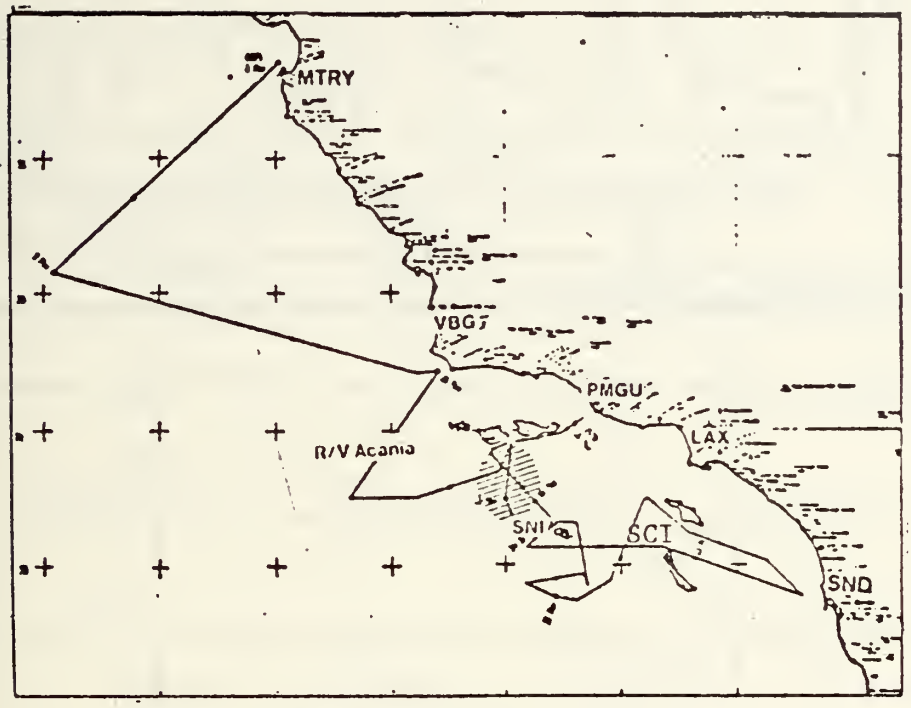

Fig. 5. Tract of R/V Acania and location of shoreline radiosonde sites during CEWCOM-78. General location of R/V Acania during 19-21 May period is indicated by hatched area N-NW of San Nicolas Island (SNI).

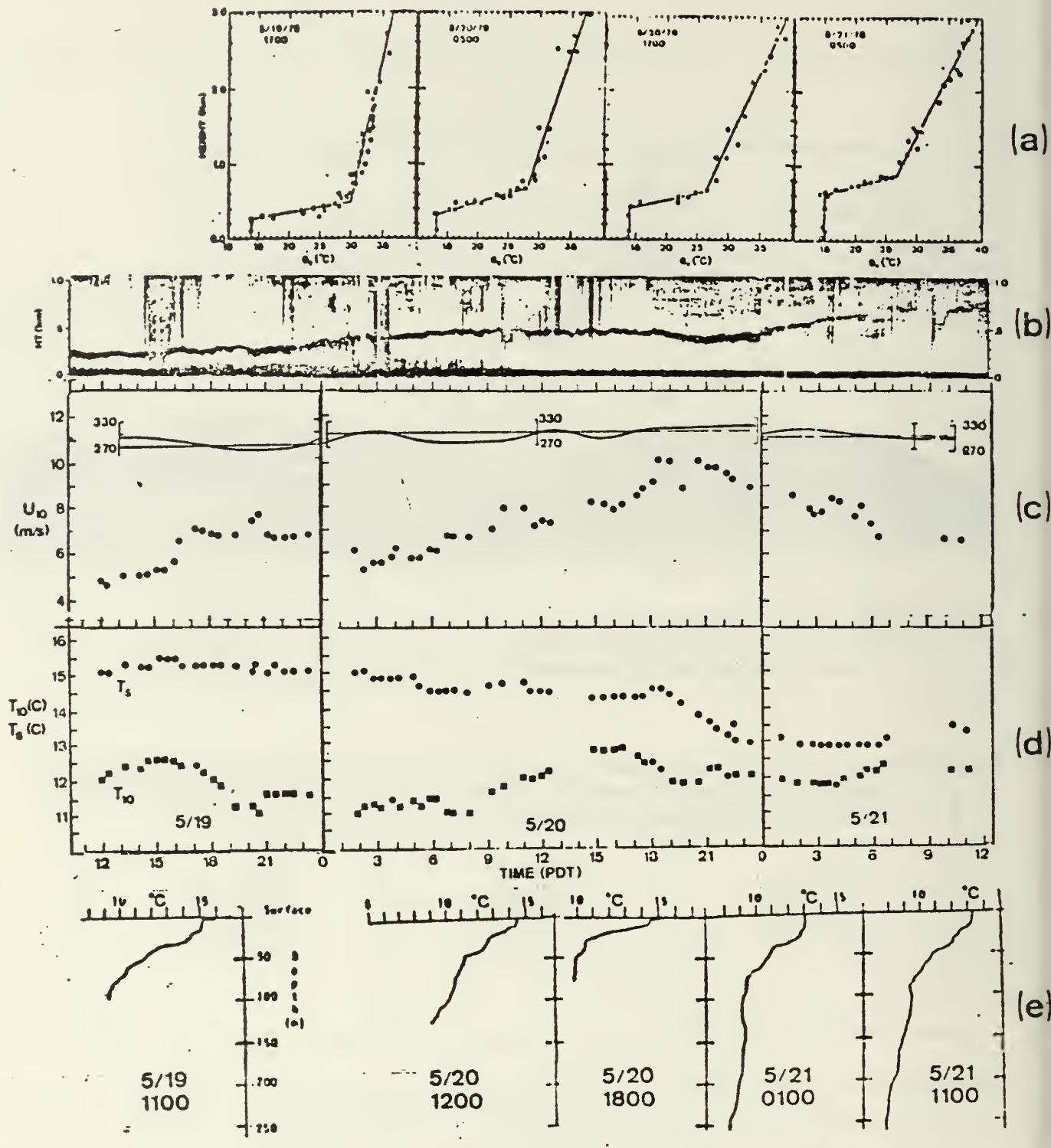

Fig. 6. Atmospheric and oceanic mixed-layer observations during CEWCOM-78 (a) potential temperature composite profiles, (b) acoustic sounder record, (c) 10 meter wind speed, (d) 10 meter and surface temperatures and (e) XBT traces.

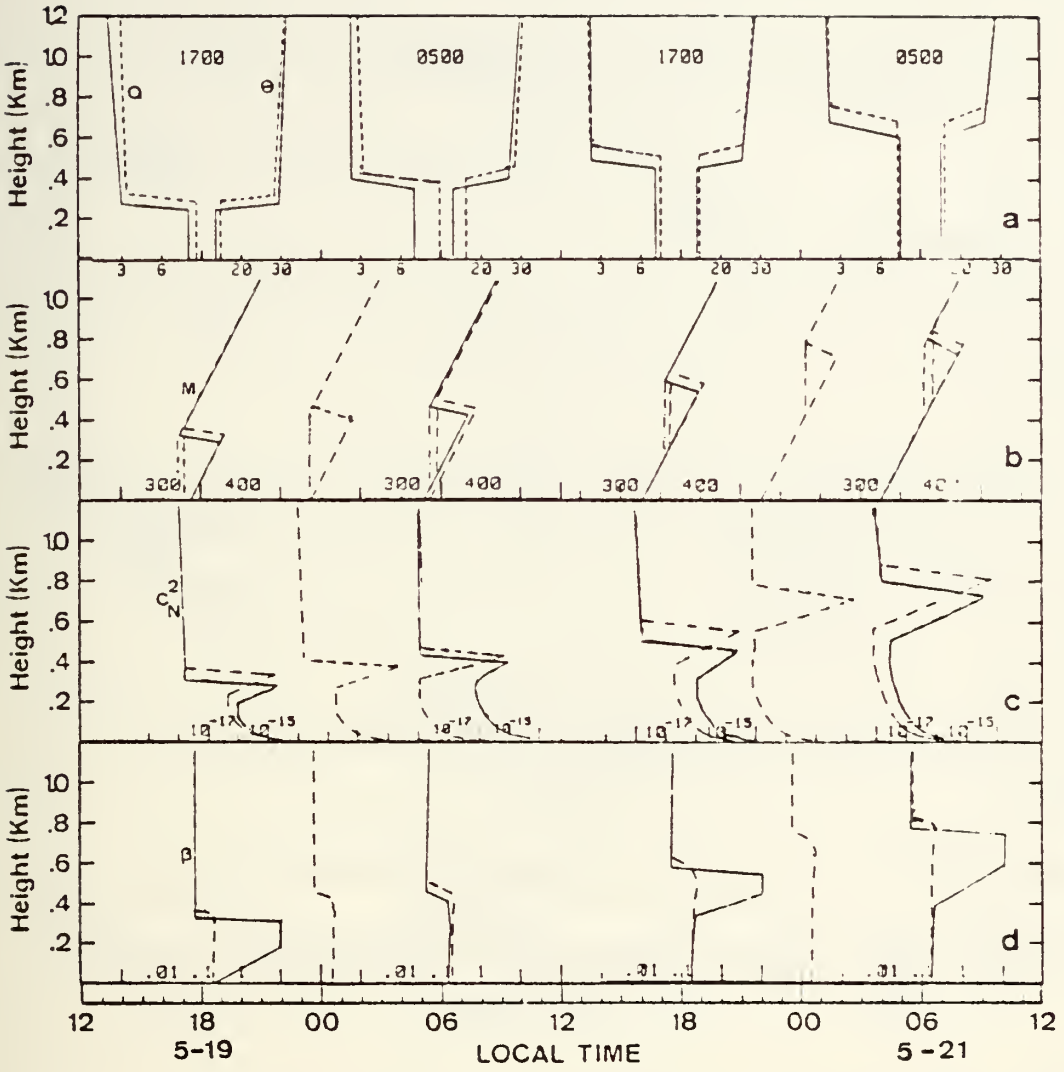

Fig. 7. Observed/computed and predicted MABL profiles for 5/19/1200 to 5/21/1200 CEWCOM-78 period including (a) Q ($g\ m^{-3}$) and θ(°C), (b) M, (c) C_N^2 ($m^{-2/3}$) and (d) total extinction coefficient, β (km^{-1}). Solid lines correspond to observed and dashed to model prediction.

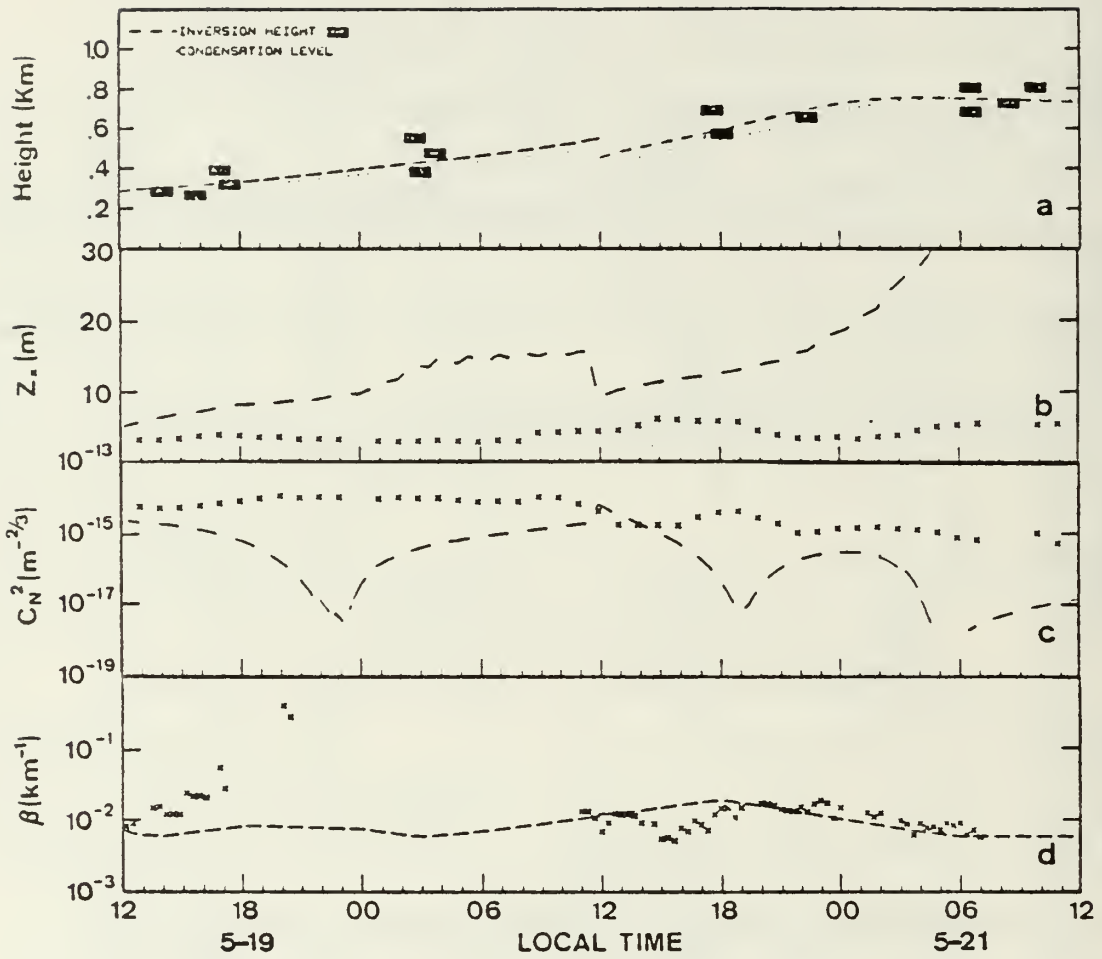

Fig. 8. Observed/computed and predicted surface layer values for 5/19/1200 to 5/21/1200 CEWCOM-78 period including (a) inversion height and lifting condensation level, (b) evaporation duct, (c) C_N^2 $m^{-2/3}$ and (d) aerosol scattering extinction coefficient, β. X's are observed and dashed lines are model predictions.

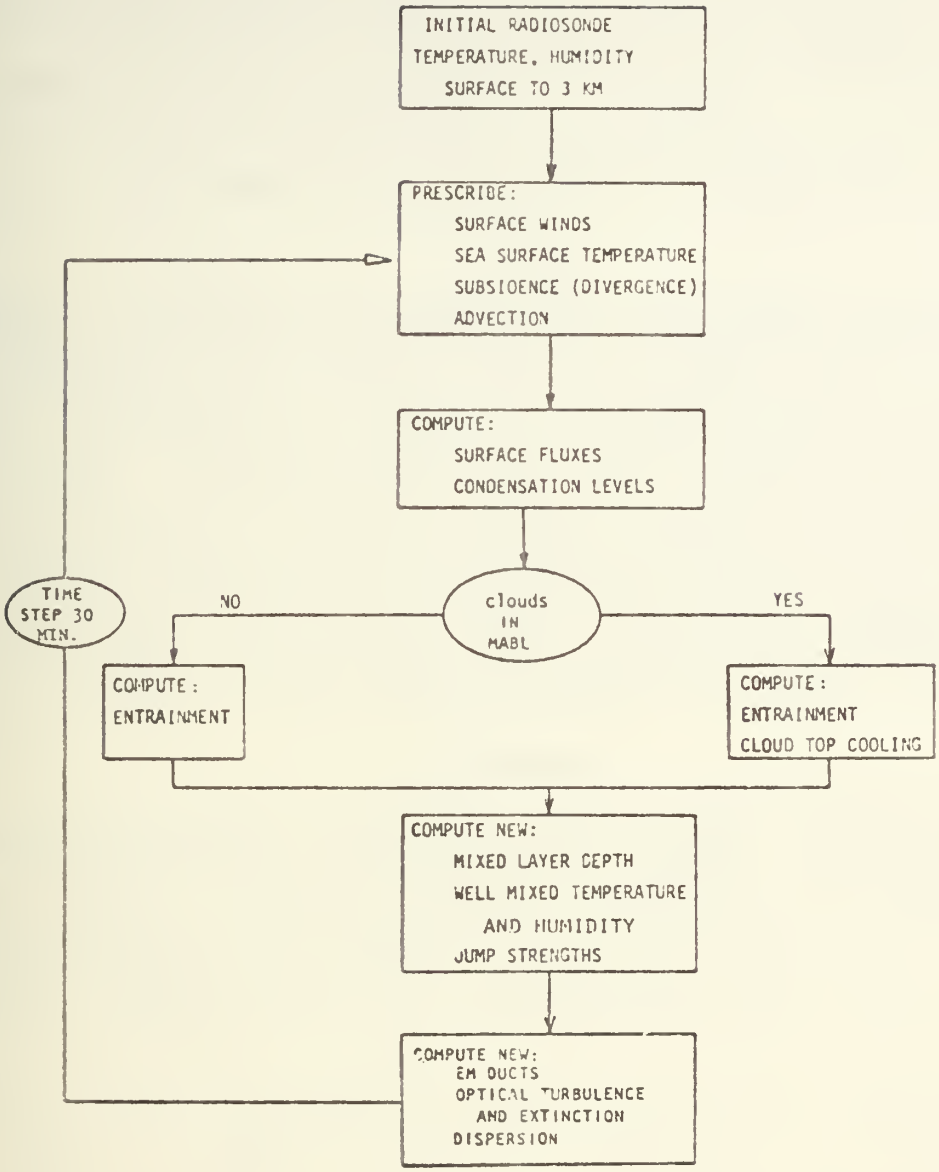

Fig. 9. Schematic of input, prescription and computing steps in MABL prediction.

Meteorological models for optical properties in the marine atmospheric boundary layer

C. W. Fairall

BDM Corporation, Naval Postgraduate School, Monterey, California 93940

K. L. Davidson and G. E. Schacher

Naval Postgraduate School, Monterey, California 93940

Abstract

Observational experiments on turbulent intensities and aerosol distributions in the marine boundary layer (MBL) have been performed over several years. Observations have been made with ship-mounted and airplane-mounted sensors. Objectives have been to relate optical properties to meteorological descriptions which utilize scaling laws for the MBL. The approach has been to incorporate in the descriptions the surface fluxes of momentum, heat, and moisture, the processes at the inversion and the profiles within the intervening convectively mixed layer. We have found that optical turbulence parameters (C_N^2 and l_0) can be readily estimated using measured mean values of wind, temperature, and humidity with recent bulk formulae to derive the surface fluxes. These estimates appear to be more reliable than values obtained from direct (but difficult to perform) turbulence measurements. The model for obtaining the estimates was evaluated on the basis of optical C_N^2 values with good agreement. Good comparisons have been observed between extinction values obtained from transmission measurements and those obtained from calculations on measured aerosol distributions. Existing empirical formulations which related the latter to wind speed and relative humidity appear to be inadequate except for climatological purposes. This is because other influences on equilibrium aerosol distribution are not included. Reformulation of these expressions is being performed to include the height of the inversion (mixing volume) and surface fluxes (aerosol generation and transport).

Introduction

Three atmospheric processes are primarily responsible for the degradation of the transmission of optical images and electro-optical energy: aerosol extinction, molecular extinction, and turbulent distortion (scintillation and beam wander). Optical energy propagating through the atmosphere is scattered and absorbed by aerosols and molecules and optical wave fronts are deflected and distorted by turbulent fluctuations in the refractive index. Tested physical models of these atmospheric effects and approaches to estimate them from routine meteorological data are required for applications of optical and electro-optical systems. Naval Postgraduate School (NPS) investigators have participated in field experiments designed to improve and verify such models and approaches for the overwater regime. These have been performed for U. S. Navy research programs over the past seven years.

The two atmospheric optical parameters of primary interest are the total extinction coefficient and the refractive-index structure function parameter, C_N^2. The total extinction coefficient ($\beta + \alpha$) parameterizes the loss of optical energy as it is scattered out of the beam or absorbed by molecular and particulate constituents of the atmosphere. Thus, it has four components: molecular scattering and absorption ($\beta = \beta_a + \beta_s$) and aerosol scattering and absorption ($\alpha = \alpha_a + \alpha_s$). The refactive-index structure function parameter parameterizes the intensity of refactive-index spatial inhomogeneities which distort and tilt image wave fronts. Both of these parameters can be related to meteorological parameters: 1) C_N^2 to the intensity of small scale turbulent fluctuations and 2) total extinction to the concentration of certain gases and to the size distribution of aerosols.

One part of the experiments dealt with the compatibility of optical and meteorological propagation theories. For this, direct optical measurements of extinction and scintillation across an overwater path were compared to values calculated from aerosol and turbulence data obtained at the midpoint of the optical path from an instrumented research vessel. Once these relationships are validated, optical properties can be deduced from detailed meteorological measurements and models.

A second part of the experiments involved attempts to apply existing models for the marine atmospheric surface layer and mixed layer to describe the optically relevant turbulent and aerosol properties. The surface layer is considered to be the region extending from the air-sea interface to heights of 40-50 meters. Its mean and turbulent properties are closely related to surface fluxes of momentum, temperature and moisture, and hence, the air-surface (bulk) differences of mean properties. The fluxes themselves are often assumed

to be independent of height within the surface layer. The mixed layer extends from the top of the surface layer to the base of the capping inversion. Properties of the mixed layer are determined by both the underlying surface fluxes and entrainment at the inversion. Fig. 1 illustrates the meteorological signature characteristic of the marine boundary layer (MBL). A well-mixed property (in this case, virtual potential temperature and water vapor mixing ratio) has a gradient in the surface layer, is constant in the mixed layer (up to height, h) changes abruptly in the interfacial layer (thickness, h) and acquires a fairly constant gradient (lapse rate, Γ) in the free troposphere. This structure prevails over the open ocean a majority of the time, the most common exception being during periods of frontal passage. This structure is due to turbulent processes driven by the air-sea interaction. These same processes lend themselves to scaling law parameterizations that allow the development of physical models of turbulence and aerosol profiles in the MBL.

Comparison of optical and meteorological values for C_N^2 and aerosol scattering extinction coefficient

C_N^2 for optical wavelengths is related to the temperature (C_T^2), water vapor (C_Q^2) and temperature-water vapor (C_{TQ}) structure function parameters by[1]

$$C_N^2 = (79 \times 10^{-6} P/T^2)^2 (C_T^2 + 0.113 C_{TQ} + 3.2 \times 10^{-3} C_Q^2) \quad (1)$$

where P is the pressure in mb, and T the absolute temperature.

The separate components of total extinction ($\beta + \alpha$) can be calculated from meteorological data. Molecular extinction (β) can be obtained using existing models, such as the LOWTRAN model developed by the Air Force Geophysics Laboratory[2], with observed temperatures and water vapor concentrations. Aerosol total extinction (α) can be calculated from the aerosol spectral density, N(r), as

$$\alpha = \int \pi r^2 E(n,\lambda) N(r) dr \quad (2)$$

where r is the particle radius, $E(n,\lambda)$ the total scattering efficiency at wavelength, λ, and refractive-index, n.

A series of field experiments to establish the credibility of Eq. 1 and Eq. 2 for practical determination of optical properties culminated in the MAGAT experiment in Monterey. Since the results have been reported for C_N^2 by Davidson et al[3] and for aerosols by Schacher et al[4], a brief summary only will be presented here.

The optical measurements were made over a 13 km overwater path and are described by Crittenden et al[5]. The meteorological measurements were made from the R/V Acania (operated by the Department of Oceanography of NPS) which was stationed near the midpoint of the optical path. The R/V Acania was equipped with multi-level measurement systems to measure mean and turbulent wind, temperature and humidity and aerosol size distribution (.09 μm to 14 μm radius). Descriptions of the measurement and analyses systems and procedures are given by Schacher et al[4]. Two measurements requiring further description for these camparisons are those of the temperature structure function parameter, C_T^2, and of the aerosol size distributions.

Meteorological values for C_N^2 in this comparison were determined primarily from C_T^2 measurements with minor (less than 15%) adjustments for the water vapor contributions, C_{TQ} and C_Q^2. The C_T^2 measurements were made with two resistance wires, 2.5 μm platinum sensors, separated a distance of 30 cm in the crosswind direction. C_T^2 values were obtained from RMS values of the sensed temperature differences.

The aerosol spectra were measured with optical particle counters made by Particle Measurement Systems (PMS) of Boulder, Colorado. The total system consisted of two probes, the classical scattering (CSAS) and the active scattering (ASAS), controlled by a DAS-32 with computer interfacing. This system measures aerosols in 90 size channels from 0.09 μm to 14.0 μm radius. The N(r) spectra were determined for half-hour periods. Each spectrum was fit in LOG(N(r)), LOG (r) space with a seventh order polynomial for $0.09\ \mu m < r < 7\ \mu m$, with a linear fit for $r > 7\mu m$. The extinction was then calculated using these fits for $0.03\ \mu m < r < 30\ \mu m$.

Comparisons of optically measured C_N^2 with meteorologically measured C_N^2 (calculated from C_T^2 measurement with correction for probable water vapor contributions) are shown in Figure 2. The salt loading effect increases measured C_T^2 values for general conditions during these measurements. The extinction comparisons are shown in Fig. 3.

Turbulence modeling

At any given point in the atmosphere, the turbulence properties are determined by the physical processes dominating that region of space. Identifying the important physical parameters and neglecting the unimportant forms the basis of the scaling law approach. As an extreme example, clearly the sea surface temperature has little influence on the turbulence at an altitude of 30 km. Therefore, the MBL is loosely partitioned into regions in which certain scaling regimes apply; these regions are summarized in Table 1. (symbols will be defined in the text).

Table 1. C_N^2 scaling regions of the MBL

region	height	relevant parameters	scaling parameters	model
surface	$Z<0.1h$	surface fluxes	$u_*, T_*, Q_*, Z/L$	bulk
free convection	$0.1h<Z<0.5h$	surface fluxes, h	$W_*, \theta_*, M_*, Z/h$	mixed layer
transition	$0.5h<Z<h$	?	---	---
interfacial	$h<z<(1+\alpha)h$	jumps, fluxes, h	W_*, W_e, α	entrainment
free troposhere	$z>(1+\alpha)h$	?	---	---

Surface layer

Monin-Obuhkov scaling (MOS). Near the surface, the height above the surface, Z, can be normalized by the Monin-Obuhkov stability length, L. We can then represent the relevant micrometeorological properties in terms of height (Z), scaling parameters (T_*, Q_* and u_*) and dimensionless functions of $\xi = Z/L$,

$$C_T^2 = T_*^2 Z^{-2/3} f(\xi) \quad (3a)$$

$$C_Q^2 = Q_*^2 Z^{-2/3} A f(\xi) \quad (3b)$$

$$C_{TQ} = r_{TQ} T_* Q_* Z^{-2/3} A^{1/2} f(\xi) \quad (3c)$$

where T_* and Q_* are the temperature and humidity scaling parameters, $f(\xi)$ is a dimensionless function[7], r_{TQ} is the temperature-humidity correction parameter (about 0.8) and A is a constant (about 0.6). The scaling length, L, is given by

$$L = (T/\kappa g)\, u_*^2/(T_* + 0.61\, TQ_*/\rho) \quad (4)$$

where u_* is the friction velocity, κ is Von Karman's constant (0.35), g is the acceleration of gravity and ρ is the density of air. Note that the scaling parameters are related to the surface fluxes of momentum ($\tau = \rho u_*^2$), temperature ($Q_o = -u_* T_*$) and water vapor ($M_o = -u_* Q_*$).

Bulk model. Using Eq. 1 and Eq. 3 one can calculate C_N^2 at some height Z in the surface layer, provided values of T_*, Q_* and L are known. The most straightforward method of obtaining these variables is to measure the surface fluxes of momentum, heat and water vapor. The difficulty of direct flux measurements led to the development of a method that utilizes bulk meteorological quantities (wind speed, u, temperature, T, and water vapor density, Q). In this case, the scaling parameter for $X (X = u, T, Q)$ is obtained from the difference in X from the sea surface (X_s) to some reference height (usually 10 m) in the atmosphere.

$$X_* = c_x^{1/2}(X_{10} - X_s) \quad (5)$$

where c_x is the drag coeficient for X (typically, $c_x = 1.3 \times 10^{-3}$ over the ocean). Further details on use of the bulk method can be found in Davidson et al [8].

The verification of the bulk method for C_T^2 and Eq. 3a is shown [8] in Fig. 4a while the corresponding verification for C_Q^2 and Eq. 3b is shown[9] in Fig. 4b. Following this work, the MAGAT experiment was performed to verify the bulk predictions against direct optical (scintillation) measurements [3] (Fig. 5).

In this comparison all but three of 26 pairs of values are within a factor of two of perfect agreement. The mean percent error, taking the optical values to be correct, is 33% which is extremely good agreement. This agreement is better than that obtained in the comparison with C_N^2 derived from C_T^2 measurements. Such a result is partially expected because of inherent measurement errors in the latter.

Results of these comparisons and results of comparison of bulk and turbulence derived parameters in the above referenced papers clearly demonstrates that surface layer optical turbulence, C_N^2, is very satisfactorily described by existing bulk formulae and scaling expressions. In fact, over the ocean C_N^2 can be more accurately determined from bulk model calucations than from the more difficult direct measurements of small scale temperature and humidity fluctuations.

Mixed Layer.

Free Convection Layer. In the lower half of the mixed layer free convection scaling applies [10, 11]; the scaling parameters are (where $Q_{ov} = Q_o + 0.61TM_o/\rho$)

$$\theta_* = Q_o/W_* \tag{6a}$$

$$M_* = M_o/W_* \tag{6b}$$

$$W_* = (gQ_{ov}h/T)^{1/3} \tag{6c}$$

Note that some authors use the height of the inversion, $Z_i = (1 + \alpha/2)h$, rather than the height of the well-mixed layer, h. Normally, Z_i is about 10% greater than h.

In this regime, the structure functions are calculated using [12]

$$C_T^2 = \theta_*^2 \, h^{-2/3} \, (Z/h)^{-4/3} \, B \tag{7a}$$

$$C_Q^2 = M_*^2 h^{-2/3} \, (Z/h)^{-4/3} AB \tag{7b}$$

$$C_{TQ} = r_{TQ} \, M_* \theta_* h^{-2/3} \, (Z/h)^{-4/3} \, A^{1/2} B \tag{7c}$$

As has been pointed out by Panofsky [13], Eq. 7 is an extension of Eq. 3 for $|Z/L| >> 1$. Thus, the matching of the surface layer-free convection layer scaling requires that B = 2.7, which has been verified by measurements [12].

Transition Layer. For $Z \gtrsim 0.5h$, Eq. 7 begins to breakdown. The actual height limit of the validity of free convective scaling depends on conditions, most notably the value of h. Basically, the greater h, the larger the value of Z/h that Eq. 7 can be used. The behavior of C_T^2 in the transition layer has been examined using an additional dimensionless function [14, 15] G(Z/h)

$$C_T^2 = \theta_*^2 \, h^{-2/3} \, (Z/h)^{-4/3} B \, G(Z/h) \tag{8}$$

Three examples of G(Z/h) are shown in Fig. 6, where it is clear that G(Z/h) is not a universal function. Since turbulence in the transition layer is influenced by the transport of turbulence from the interfacial layer, it is likely that scaling in the region will require "matching" with the entrainment scaling.

Interfacial Layer. Turbulence at the top of the mixed layer erodes the interface separating the turbulent boundary layer and the quiescent , stable air of the free troposphere. The rate of this process, which is called entrainment, depends upon the amount of turbulence available and the amount of work the turbulence must do to erode the boundary. The amount of turbulence is generally a function of the surface fluxes and the mixing velocity, W_*. The barrier the turbulence works against is primarily a function of the bouyancy jump, $\Delta\theta_v$ and the lapse rate, Γ_T, of the upper layer. The mixing in of the warm, dry air from above the inversion creates considerable fluctuation in temperature and water vapor with a resultant large increase in C_T^2, C_Q^2, and C_{TQ}.

Using Deardorff's [16] model of the interfacial region, Wyngaard and LeMone [12] have developed a model to predict the structure functions

$$C_T^2 = \Delta\theta_v \, (1 + \alpha)\Gamma_T h^{1/3} \, (W_e/W_*) F_{TT} \tag{9a}$$

$$C_Q^2 = 4(\Delta Q)^2 (1 + \alpha)\Gamma_T h^{1/3} (W_e/W_*)/\Delta\theta_v \tag{9b}$$

$$C_{TQ} = \Delta Q (1 + \alpha)\Gamma_T h^{1/3} \, (W_e/W_*) F_{TQ} \tag{9c}$$

where ΔQ is the jump in water vapor density (remember that ΔQ is negative!), W_e is the entrainment rate (m/s), F_{TQ} and F_{TT} are functions that relate virtual temperature fluctuations to the temperature fluctuations [12].

The final step in obtaining a structure function formulation is to select a parameterization of W_e. Wyngaard and LeMone chose the second order entrainment model equilibrium rate[16]

$$W_e = 0.8 \, Q_{ov}/((1 + \alpha) \, \Gamma_T h) \tag{10}$$

and obtain excellent agreement with NCAR aircraft data. A much more common assumption is that [17]

$$W_e = 0.2 Q_{ov}/\Delta\theta_v \tag{11}$$

In fact, the major uncertainty in the application of Eq. 9 is the entrainment energy (bouyancy, surface shear, inversion shear, and atmospheric waves) and dozens of entrainment relationships[18] exist. Another problem is the appropriate value of the interface thickness, α. Typical values of α range from 0.1 to 0.5 with an average of 0.3. Also, since α represents an ensemble average property, a single measurement (by a radiosonde, for instance) may not give an accurate estimate. Note that if Eq. 10 is used, α and Γ_T, drop-out of the structure function calculation (Eq. 9). Another source of error in the Wyngaard and LeMone model is the assumption that the average rate of dissipation of turbulent kinetic energy, ε_i, in the interfacial layer is simply one half the free convection prediction

$$\varepsilon_i = 1/2\ \varepsilon_{fc} = 0.2\ gQ_{ov}/T \qquad (12)$$

Since the C_N^2 prediction is proportional to $\varepsilon^{-1/3}$, an underestimate of ε_i would lead to an overestimate of C_N^2. Thus, wind shear at the inversion not only leads to an underestimate of W_e but also to an underestimate of ε_i (note that these two errors tend to compensate). A summary of four cloud-free measurements in the interfacial layer made during the MAGAT experiment[19] is shown in Table 2.

Table 2. Boundary layer and interfacial layer data from four MAGAT aircraft profiles

Date	4/3	5/4	5/4	5/7
Time, PST	1610	1024	1201	1043
h, m	320.00	300.00	330.00	200.00
α	.35	.5	.5	.5
$\Delta\theta_v$, K	6.5	11.00	9.00	7.00
ΔQ, g/m^3	-4.4	-5.2	-5.2	-2.00
Q_{ov}, Km/s	.027	.022	.02	.02
Γ_T, K/km	9.00	10.00	15.00	9.00
W_*, m/s	.65	.6	.7	.5
$\varepsilon_i^{1/3}$, m$^{2/3}$/s	.13	.06	.12	.067
$(0.2g\ Q_{ov}/T)^{1/3}$, m$^{2/3}$/s	.056	.053	.052	.052
F_{TT}	.90	.78	.86	.66
$C_{T_i}^2$, K^2/m$^{2/3}$	3.4×10^{-3}	7.3×10^{-4}	3.8×10^{-3}	6.0×10^{-3}
$C_{Q_i}^2$, (g/m^3)^2/m$^{2/3}$	9.6×10^{-3}	1.8×10^{-3}	6.4×10^{-3}	1.9×10^{-3}

Table 3 compares the measured structure functions with the Wyngaard and LeMone model using Eq. 10 and Eq. 11.

Table 3. Comparison of MAGAT interfacial structure function data with entrainment model predictions

Source	$\langle C_T^2 \rangle$, K^2/m$^{2/3}$	$\langle C_Q^2 \rangle$, (g/m^3)^2/m$^{2/3}$
Measurements	3.5×10^{-3}	4.9×10^{-3}
$W_e = 0.8\ Q_{ov}/((1+\alpha)\Gamma_T h)$	4.5×10^{-3}	5.6×10^{-3}
$W_e = 0.2\ Q_{ov}/\Delta\theta_v$	0.6×10^{-3}	0.7×10^{-3}

Free troposphere

Except in regions of clear air turbulence (CAT), C_N^2 in the free troposphere is quite small. Typical values of C_T^2 are on the order of 10^{-5} K^2/m$^{2/3}$, leading to $C_N^2 \approx 5 \times 10^{-18}$ m$^{-2/3}$ at Z = 5km. The decrease of atmospheric pressure with increasing altitude is another factor that reduces C_N^2 relative to C_T^2 (Fig. 7). There are measurements in this region [20,21,22,23,24] but there are no physical models. There are several phenomenological models [21,25] that relate C_T^2 to local temperature vertical gradients. A good review of the subject is given by Hall[26].

Aerosol modeling

Given the validity of the micrometeorological relationship of molecular and aerosol extinction to actual optical extinction, the optical model is considered to be equivalent to the meteorological. For molecular extinction, the pressure, temperature and relative humidity are obtained within the framework of the MBL structure as depicted in Fig. 1. Thus, surface layer measurements of temperature, relative humidity, plus the height, h, are sufficient to calculate the molecular extinctions (using LOWTRAN) throughout the MBL. If, in addition, a surface layer measurement of the aerosol spectrum is available, then it is also possible to calculate the aerosol extinction profile throughout the MBL using an aerosol mixed layer structure which we shall describe. Although temperature and humidity are easily available over the ocean, routine measurements of aerosol spectra are most certainly far in the future. Thus, it is necessary to develop a model which allows estimates of the aerosol spectrum from routinely available oceanic meteorological data. The remainder of this section will be devoted to the aerosol problem since the molecular is

considered to be, by comparison, more than adequately solved.

Aerosol basics

Before attacking the aerosol MBL problem, it is necessary to establish some general background in marine aerosols.

Relative humidity. It is well known that aerosol particles over the ocean are usually in the form of dissolved or coated droplets. The size of these droplets changes as liquid water is absorbed or lost in response to its relative humidity variations[27]. For example, let r_o be the particle radius at some reference water vapor saturation S_o($S = RH/100$) and r be the particle radius at ambient saturation S, then

$$r = r_o\, g(S) \tag{13}$$

where (assuming $S_o = 0.8$)

$$g(S) = 0.81 \exp(0.066\, S/(1.058 - S)) \tag{14}$$

This relation is particularly useful because one can eliminate variations of the aerosol spectrum due solely to humidity variations by dealing with the spectrum as it would appear at the reference humidity. Thus, if N(r) is the ambient aerosol number density, we can transform N(r) to the reference saturation spectrum $N(r_o)$,

$$N(r/g(S)) = N(r_o) = N(r)\, g(S) \tag{15}$$

Since some of the results to be described are in aerosol volume format, $V(r) = 4/3\pi r^3\, N(r)$, the equivalent volume relation should be considered

$$V(r/g(S)) = V(r_o) = V(r)/g^2(S) \tag{16}$$

Aerosol spectrum components. Over the ocean, the aerosol spectrum at small sizes ($r < 1.0$ μm) is dominated by particles of nonlocal origin (continental background) while the larger sizes ($r > 1.0$ μm) are primarily sea salt droplets produced by whitecaps. Since particles with radius less than 0.1 μm do not contribute significantly to extinction at visible and IR wavelengths, the continental aerosols can be reasonably represented by the Junge distribution

$$V_c(r_o) = A/r_o \tag{17}$$

If we define $V_s(r_o)$ as the sea salt component, then the total aerosol spectrum in the MBL is

$$V(r_o) = V_s(r_o) + V_c(r_o) \tag{18}$$

Accurate broad band aerosol spectrum measurements can be used to determine the continental influence by assuming that at $r_o = 0.1$ μm, $V_s(0.1) = 0$ and therefore

$$A = 0.1\, V_c(0.1) = 0.1\, V\,(0.1) \tag{19}$$

This assumption is corroborated by aerosol data taken in the North Atlantic (JASIN experiment) that has been averaged in ensembles based on wind speed (Fig. 8). The lack of wind speed dependence of the aerosol volume at $r_o = 0.1$ μm demonstrates that these particles are primarily of continental origin. The average value of A obtained was 1.0. The claim that A is an index of continental influence is further validated by a comparison of NPS values of A with atmospheric Radon activity obtained by NRL[28] during CEWCOM-78 (Fig. 9). Given a measurement of A, one can now calculate the sea salt aerosol spectral component

$$V_s(r_o) = V(r_o) - A/r_o \tag{20}$$

One note of caution: in order to be consistent with the literature, we will use aerosol coefficients A and B; these bear no relation to A and B in the section on turbulence.

Aerosol MBL structure

The necessity for the partitioning of aerosol components becomes clear when one considers the different particle sources they represent. Because sea salt particles are produced by whitecaps at the sea surface, they tend to remain trapped within the MBL. Thus we assume $V_s = 0$ for $Z > h$. Continental aerosols are assumed to be distributed with approximately constant mixing ratio both above and below the MBL. The vertical structure being proposed is depicted in Fig. 10. Recall that we are describing the aerosol density at reference

saturation, $S_o = 0.8$. Since the saturation tends to increase with increasing altitude in the MBL (this is consistent with Fig. 1 where θ_v and dewpoint are nearly constant, therefore T must decrease roughly one degree per hundred meters), the actual measured spectrum (or extinction coefficient) will tend to increase.[29,30] Conversely, if one takes a measured vertical profile of aerosol volume and removes the humidity dependence using Eq. 16, then the reference humidity aerosol volume is nearly height independent in the MBL (Fig. 11). Note the aerosol volume decreased rapidly above the MBL indicating that, in this case, most of the volume in the MBL is due to sea salt particles.

Surface layer gradient. One issue not covered in the structure shown in Fig. 10 is the near surface vertical gradient. Since continental aerosols are not surface produced, they do not have significant near surface gradients. In the case of sea salt aerosols, the surface gradient is produced by a near balance of turbulent upward transport of particles and the gravitational (Stokes fallout) downward transport.[31,32] For particles in the 0.1 μm to 15 μm range, this gradient is very small at heights greater than a few meters and probably not worth further consideration (except for long wavelength, near surface IR applications).

Scaling law perspective. The development of physical scaling equations for aerosols is somewhat simpler than for C_N^2 because one is not modeling the fluctuations but rather the mean aerosol profile. Thus, the aerosol model is roughly analogous to the mean profile of water vapor - there is surface production (evaporation) and continental background (water vapor advected over the ocean) which is present above and below the MBL. Unlike the C_N^2 case, however, the surface layer aerosol density cannot be "a priori" calculated without consideration of mixed layer processes (this is also true of the mean water vapor density). This will be discussed in later sections.

The Wells-Munn-Katz (WMK) model

The present state-of-the-art in bulk aerosol models is represented by the WMK model[33,34] where the continental component is the Junge type (Eq. 17).

$$N_c(r) = B/r_o^4 \tag{21a}$$

$$B = 3A/(4\pi) \tag{21b}$$

and the sea salt component has a wind speed and height dependence of the gamma function form[29]

$$N_s(r) = F(r_o,u)\ \exp(-Z/h_o) \tag{22}$$

($r_o = r/g(S)$ as in Eq. 13 and Eq. 14).

The exponential decay with scale height, $h_o = 800$m, though in clear disagreement with the well-mixed assumption (Fig. 11), is probably adequate for some applications (satellite remote sensing, for example). Although there are ongoing efforts to improve the sea salt modeling function[35], it is certainly worthwhile to examine in detail the near surface performance of the WMK model.

WMK model evaluation using JASIN data. This evaluation is basically a comparison of WMK model predictions of aerosol extinction based on measurements of relative humidity and wind speed with extinctions obtained from measurements of aerosol spectra. A twenty minute averaging period was used for RH and aerosol spectra. The wind speed used in Eq. 22 was an average over the 12 hours preceding the aerosol data in order to take into account the long response times required for sea salt aerosol generation. This comparison (Fig. 12) asks "given a wind speed and relative humidity, how well does the model predict the observed extinction"? Clearly, the WMK model predicts very well on the average with a rather large standard deviation (about half an order of magnitude, or a factor of 3). A considerably more stringent comparison asks "given an observed extinction, how well does the model predict this extinction"? This comparison (Fig. 13) is considerably less favorable, particularly in the extremes of good visibility and low visibility conditions. A certain amount of disagreement of this type is expected when comparing quantities that are subject to experimental error. However, we found that a considerable part of the discrepancy is due to overestimation of the continental aerosol component (WMK assume B = 1.7 while JASIN gives B = 0.24). If we change B to 0.24 and repeat the comparison (X's in Fig. 13), we get some improvement. Furthermore, there is considerable correlation between visible extinction and the amount of continental aerosol; the high visibility conditions have, relatively, much smaller continental aerosol densities while the low visibility-conditions have relatively greater continental aerosol densities. The disagreement at high extinction values is due to the inaccuracy of the relative humidity measurement which is critical under near fog and heavy haze conditions, where RH = 100%.

It is important to realize that the WMK model is an average continental, equilibrium surface generation model. Variations of the continental aerosol were more than an order of magnitude during JASIN. The sea salt component is also subject to considerable deviations from equilibrium (this is one of the reasons for the 12 hour average wind speeds). The deviations from average and equilibrium values are more important for operational usage and somewhat less important for climatological and spectrum evaluation usage. An example where both usages are affected is the estimation of IR extinction using visible extinctions (visibility observations) and empirical assumptions about their relationship. We have plotted the visible to IR extinction ratio in Fig. 14 with lines indicating the WMK model predictions using two different continental aerosol coefficients. Since the continental aerosol coefficients are correlated to visibility, the correct ratio depends not only on wind speed but also the visibility observation.

Although we have dealt with the stochastic properties of ensemble averages of the aerosols, variations about the average are not necessarily random but are primarily due to changes in synoptic and mesoscale weather patterns. In the case of the continental aerosol component, this is basically a question of air-mass history. In the case of the sea salt aerosol, it is a question of changing surface generation rates (wind speed) and the production, removal and mixing mechanisms in the marine atmospheric boundary layer. Since the surface generated aerosols are quickly mixed verically to fill the boundary layer up to the capping inversion, rapid changes in the inversion height, h, will be reflected in changes in the sea salt aerosol density and, therefore, the extinction coefficient. In Fig. 15 we can see that the fractional variations in h are highly correlated with variations in the visible extinction. The correlation with 10.6 μm extinction is considerably less because the large size aerosols (which are heavier contributors to IR extinction) reach equilibrium more quickly after changes in surface conditions.

The aerosol mixed-layer model

The sea surface is a continuous source of sea salt aerosols in the marine boundary layer. These surface produced aerosols can be characterized by a surface flux spectrum, $F_s(r_o)$, which represents the volume of aerosol per particle radius interval produced per square centimeter of ocean surface each second as a function of aerosol particle radius. This quantity is a function of wind speed.

The continuous production of sea salt aerosols is balanced by several removal mechanisms. One obvious mechanism is the loss of particles as they fall back to the surface. This settling under gravity is called "Stokes fallout" and is characterized by the Stokes velocity. The particles are transported vertically by turblence in the marine boundary layer and maintained at a uniform density throughout the mixed layer. The growth of the height of the layer constitutes another loss mechanism called "entrainment", which was discussed in the interfacial turbulence section of this paper. The final loss mechanism is "rainout" which occurs when the particles become condensation nuclei in the formation of clouds.

Given the surface flux spectrum and a parameterization of the removal mechanisms, one could predict evolutions of the aerosol density spectrum by the following equation[36]

$$h dV_s/dt = F_s - (W_e + W_s)V_s \tag{23}$$

where W_s is the Stokes velocity

$$W_s = 1.57 \times 10^{-2} (1 + 1.2 (0.91/g(S))^3) r_o^2 g^2(S) \tag{24}$$

where r_o is in μm, W_s is in cm/sec. In Eq. 23 we have left out the cloud formation removal mechanism because it acts on a much longer time scale. One assumption implicit in Eq. 23 is that the convective mixing velocity, W_*, is much larger than W_s. Since W_* is typically 1 m/sec while W_s is on the order of 0.1 m/sec for the largest particles (r = 15 μm) considered here, the assumption is reasonable.

The surface flux spectrum $F_s(r_o)$, which is a major factor in Eq. 23, is not well known. Some preliminary estimates are available from laboratory measurements[37]. In an effort to obtain improved information about $F_s(r_o)$, the CEWCOM-78 data have been used to evaluate the surface flux.[38] Since the other terms of the expression were measured, one simply calculates F_s using a rearrangement of the terms. Thus, the final expression for the flux calculation is,

$$F_s = h dV_s/dt + (W_e + W_s)V_s \tag{25}$$

A period was chosen from CEWCOM-78 where all data were available, the synoptic conditions were fairly constant, the wind speed was reaonably constant and a good mixed layer was present (5/20-5/21). Because of the reasonably constant wind speeds during the 20 hour CEWCOM-78 period, we were able to improve the statistical certainty for the F_s calculation

by combining all the data from the period, assuming that the flux would be a reasonable representation for U = 9 m/sec wind speed. Thus, we now have the surface flux spectrum at a single wind speed. In order to estimate the flux at other wind speeds, we note that the right hand side of Eq. 25 is nearly independent of wind speed for equilibrium conditions. Therefore, the flux at one wind speed can be related to the flux at other wind speeds if the equilibrium volume spectra are known:

$$F_s(U_1) = F_s(U_2)\ V_s(U_1)/V_s(U_2) \tag{26}$$

We have available from JASIN a large set of ensemble averages of aerosol volume spectra at different wind speeds (Fig. 16). It is a simple matter to apply this data to Eq. 26, using the CEWCOM-78 aerosol flux and equilibrium spectrum to generate the surface volume flux spectra as a function of wind speed (Fig. 17).

Equilibrium. During periods of fairly constant boundary layer conditions, the aerosol spectrum may be in a state of equilibrium (that is, $dV_s(r_o)/dt = 0$). Under these conditions, the average equilibrium spectrum is

$$\overline{V}_s(r_o) = F_s(r_o)/(W_e + W_s) \tag{27}$$

$\overline{V}_s(r_o)$, which is a function of wind speed, humidity and entrainment, is analogous to the WMK sea salt spectrum which is also for an "average" condition. Deviations of $V_s(r_o)$ from $\overline{V}_s(r_o)$ are described by Eq. 23.

Non-equilibrium. For time periods of a few hours, the aerosol spectrum may not be in a state of dynamic equilibrium. If we rewrite Eq. 23 in the following form:

$$dV_s/dt + V_s/\tau_p = F_s/h \tag{28}$$

where the time constant, τ_p, is

$$\tau_p = h/(W_e + W_s) \tag{29}$$

then we see the analogy of aerosols and a capacitor charged by an applied "voltage", F_s, through a "resistance", $(W_e + W_s)^{-1}$. In this analogy, the "capacitance", is h.

The response time of the aerosol density is a strong function of particle radius because $W_s \sim r^2$. Values of τ_p for S = 0.8 and h = 400 m are given in Table 4.

TABLE 4 The equilibrium time constant for aerosols at S = 0.8, h = 400 and W_e = 0.4 cm/s

r, μm	0.5	1	5	10	15
τ_p, hours	28	22	11	3.5	0.5

The boundary layer mixing time, τ_m, which represents the time required for changes in aerosol density to be evenly distributed throughout the marine layer is:

$$\tau_m = h/W_* \tag{30}$$

For the CEWCOM-78 analysis period (h = 400 m and W_* = 0.6 m/s) we find τ_m = .16 hours. Therefore, short term variations in mixing volume (dh/dt) will lead to changes in the aerosol density because the production response time is much slower than the mixing time. Thus, for time periods on the order of one hour, changes in the aerosol density (dV_s/dt) will be highly correlated with the mixing volume term ($h^{-1}\ V_s\ dh/dt$). The effect will be particularly noticeable for smaller particles and is the explanation for Fig. 15.

Discussion

Given the great difficulty of direct optical measurement of the propagation properties (C_N^2 and extinction vertical profiles) of the MBL, it is necessary to estimate these properties from more practical, routine atmospheric data. This is accomplished by relating the optical properties to micrometeorological quantities (turbulence, molecular constituents and aerosol spectra) where the atmospheric physical foundation exists for the development of reasonably simple scaling models. The first step in this process was to verify the optical-meteorological relationships in the marine regime. Although C_N^2 and extinction were considered separately, both models were cast in the same framework of a well mixed marine layer capped by an entraining inversion; the structure of the MBL is a key element in modeling of the height dependences above the near surface region. Since the mixing and entrainment process (also, the turbulence) are driven by the surface fluxes, the key element of this effort was the development and verification of the bulk aerodynamic method which allows calculation of the fluxes and scaling parameters from routine surface observations (sea

surface temperature, air temperature, relative humidity and wind speed). A measurement for estimation of the mixed layer height, h, will permit calculation of the profiles for most of the remaining (non-surface) MBL. Both C_N^2 (near the inversion) and aerosol spectral structure models require knowledge of the entrainment rate which necessitate at least a radiosonde estimate of the temperature and humidity discontinuities at the inversion and the free troposphere temperature lapse rate. The aerosol model also requires a specification of the continental component. At present this is an assumed climatological mean but it could be related to visibility observations or air-mass trajectory.

The accuracy of these models is very difficult to access. In the case of turbulence, the accuracy of the input data is critical. For aerosols, the variations of continental aerosols and open ocean mixed layer effects are simply not very well known. Based solely on our experience, a best guess of the RMS error of the turbulence model is about a factor of two (average over the MBL); for extinction the error is about a factor of three.

Acknowledgments

This work was supported by the following agencies of the U. S. Navy: NAVAIR (AIR 370), NAVMAT (EO/MET) and NAVSEA (HEL). The cooperation of NOSC, NEPRF and NRL is also acknowledged.

References

1. Friehe, C. A., "Estimation of the Refractive-Index Structure Parameter in the Atmospheric Boundary Layer over the Ocean," Applied Optics, Vol. 16, pp. 334-340. 1977.

2. Selby, J. E., F. X. Kneizys, J. H. Chetwynd and R. A. McClatchey, Atmospheric Transmittance/radiance: Computer Code LOWTRAN-4, Tech. Report AFGL-TR-78-0053. 1978.

3. Davidson, K. L., G. E. Schacher, C. W. Fairall and A. Goroch, "Verification of the Bulk Method for Calculation of Overwater Optical Turbulence," Applied Optics. To be published.

4. Schacher, G. E., K. L. Davidson, C. W. Fairall and D. E. Spiel, "Calculation of Optical Extinction from Aerosol Data," Applied Optics, submitted. 1981.

5. Crittenden, E. C., and E. A. Milne, A. W. Cooper, G. W. Rodeback and S. Kalmbach, Multiwavelength Extinction and Index Fluctuation Measurements, Proc. AGARD Conference, Monterey, California. 1981.

6. Fairall, C. W., K. L. Davidson and G. E. Schacher, "Humidity Effects and Sea Salt Contamination of Atmospheric Temperature Sensors," J. Appl. Meteor., Vol. 18, pp. 1237-1239. 1979.

7. Wyngaard, J. C., Y. Izumi and S. A. Collins, "Behavior of the Refractive Index Structure Parameter near the Ground," J. Opt. Soc. Am., Vol. 61, pp. 1646-1650. 1971.

8. Davidson, K. L., T. M. Houlihan, C. W. Fairall and G. E. Schacher, "Observation of Temperature Structure Function Parameter, C_T^2, over the Ocean," Bound.-Layer Meteor., Vol. 15, pp. 507-523. 1978.

9. Fairall, C. W., G. E. Schacher and K. L. Davidson, "Measurements of the Humidity Structure Function Parameters, C_Q^2 and C_{TQ}, over the Ocean," Bound.-Layer Meteor., Vol. 19, pp. 81-89. 1980.

10. Kaimal, J. C., J. C. Wyngaard, D. Haugen, O. R. Cote and Y. Izumi, "Turbulence Structure in the Convective Boundary Layer," J. Atmos. Sci., Vol. 33, pp. 2152-2169. 1976.

11. Wyngaard, J. C. W. T. Pennell, D. H. Lenschow and M. A. LeMone, "The Temperature Humidity Covariance Budget in Convective Boundary Layer," J. Atmos. Sci., Vol. 35, pp. 47-58. 1978.

12. Wyngaard, J. C. and M. A. LeMone, "Behavior of the Refractive Index Structure Parameter in the Entraining Convective Boundary Layer," J. Atmos. Sci., Vol. 37, pp. 1573-1585. 1980.

13. Panofsky, H. A., "Matching in the Convective Planetary Boundary Layer," J. Atmos. Sci., Vol. 35, pp. 272-276. 1978.

14. Frisch, A. S. and G. R. Ochs, "A Note on the Behavior of the Temperature Structure Parameter in a Convective Layer Capped by a Marine Inversion," J. Appl. Meteor., Vol. 14, pp. 415-419. 1975.

15. Fairall, C. W., Ralph Markson, G. E. Schacher and K. L. Davidson, "An Aircraft Study of Turbulence Dissipation Rate and Temperature Structure Function in the Unstable Marine Atmospheric Boundary Layer," Bound.-Layer Meteor., Vol. 19, pp. 453-469. 1980.

16. Deardorff, J. W., "Prediction of Convective Mixed-Layer Entrainment for Realistic Capping Inversion Structure," J. Atmos. Sci., Vol. 36, pp. 424-436. 1979.

17. Stull, Roland B., "The Energetics of Entrainment Across a Density Interface," J. Atmos. Sci., Vol. 33, pp. 1260-1267. 1976.

18. Deardorff, J. W., Progress in Understanding Entrainment at the Top of a Mixed Layer, Proc. AMS Workshop on the Planetary Boundary Layer, Boulder, Colorado. 1978.

19. Fairall, C. W., G. E. Schacher and K. L. Davidson, Atmospheric Optical Propagation Comparisons during MAGAT-80, Tech. Report NPS-61-81-002. 1981.

20. Koprov, V. N. and L. R. Tsvang, "Characteristics of Very Small-Scale Turbulence in a Stratified Boundary Layer," Atmos. and Oceanic Phys. (USSR), Vol. 22, pp. 1142-1150. 1966.

21. Bufton, J. L., "Comparison of Vertical Profile Turbulence Structure with Stellar Observations," Applied Optics, Vol. 12, pp. 1785-1793. 1973.
22. Lawrence, R. S., G. R. Ochs and S. F. Clifford, "Measurements of Atmospheric Turbulence Relevant to Optical Propagation," J. Opt. Soc. Am., Vol. 60, pp. 826-830. 1970.
23. Collins, S. A., Y. J. Liu, and L. E. Pape, Altitude Dependence of C Evaluation of Airborn Refractive Index Fluctuations, Proc. of Optical Propagation through Turbulence, Rain and Fog, Boulder, Colorado. 1977.
24. Hanson, Donald W., Atmospheric Turbulence Measurements at AMOS, Proc. Optical-Submillimeter Atmospheric Propagation Conference, Colorado Springs, Colorado, pp. 245-254. 1976.
25. Yura, H., Interim Report for ARPA, order 2843, SAMOS TR. Unpublished.
26. Hall, Freeman, F., Index of Refraction Structure Parameter in the Real Atmosphere - An Overview, Proc. Optical Propagation through Turbulence, Rain and Fog, Boulder, Colorado. 1977.
27. Fitzgerald, James W., "Approximation Formulas for the Equilibrium Size of an Aerosol Particle as a Function of its Dry Size and Composition and the Ambient Relative Humidity," J. Appl. Meteor., Vol. 14, pp. 1044-1049. 1975.
28. Larsen, R. E., W. Kasemir and D. J. Bressan, Measurements of Atmospheric Radon at San Nicolas Island and over nearby California Coastal Areas during CEWCOM-78, Tech. Report NRL 3941. 1979.
29. Hughes, H. G. and J. H. Richter, "Extinction Coefficients Calculated from Aerosol Size Distributions Measured in a Marine Environment," Optical Engineering, Vol. 19, pp. 616-620. 1980.
30. Johnson, R. W. and W. S. Hering, Measurements of Optical Atmospheric Quantities in Europe and their Application to Modelling Visible Spectrum Contrast Tranmittance, Proc. 29th AGARD Symposium on EM Propagation, Monterey, California. 1981.
31. Toba, Y., "On the Giant Sea-Salt Particles in the Atmosphere; II. Theory of the Vertical Distribution is the 10 m Layer over the Ocean," Tellus, Vol. 17, pp. 365-382.
32. Goroch, Andreas, Stephen Burk and K. L. Davidson, "Stability Effects on Aerosol Size and Height Distributions," Tellus, Vol. 32, pp. 245-250. 1980.
33. Wells, W. C., G. Gal and M. W. Munn, "Aerosol Distribution in Maritime Air and Predicted Scattering Coefficients in the Infrared," Applied Optics, Vol. 16, pp. 654-659. 1977.
34. Noonkester, V. R., Offshore Aerosol Spectra and Humidity Relations near Southern California, Proc. 2nd Coastal Meteorology Conference, Los Angeles, California, pp. 113-120. 1981.
35. Goroch, Andreas K., C. W. Fairall and K. L. Davidson, "Modelling Wind Speed Dependence of Marine Aerosol Distributions by a Gamma Function," J. Appl. Meteor., submitted. 1981.
36. Davidson, K. L., C. W. Fairall and G. E. Schacher, "A Mixed Layer Model of the Dynamics of the Marine Aerosol," Tellus, in preparation. 1981.
37. Monahan, E. C., B. D. O'Regan and D. M. Doyle, The Influence of Whitecaps on the Marine Atmosphere, Annual Report for ONR, University College, Galway, Ireland. Unpublished.
38. Fairall, C. W., K. L. Davidson and G. E. Schacher, "An Analysis of the Surface Production of Sea-Salt Aerosols," Tellus, submitted. 1981.

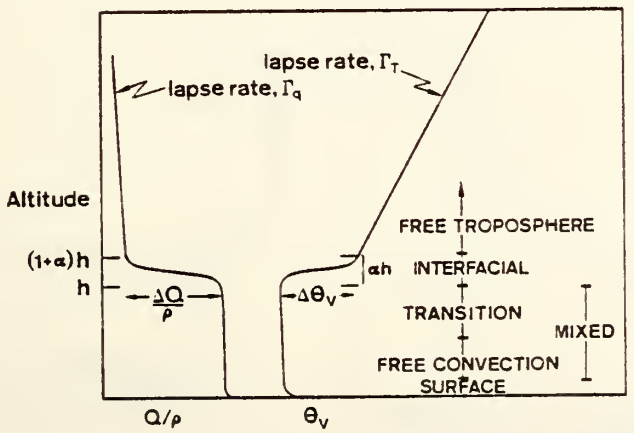

Figure 1 Typical structure of the marine atmospheric boundary layer in terms of water vapor density, Q, and virtual potential temperature, θ_v.

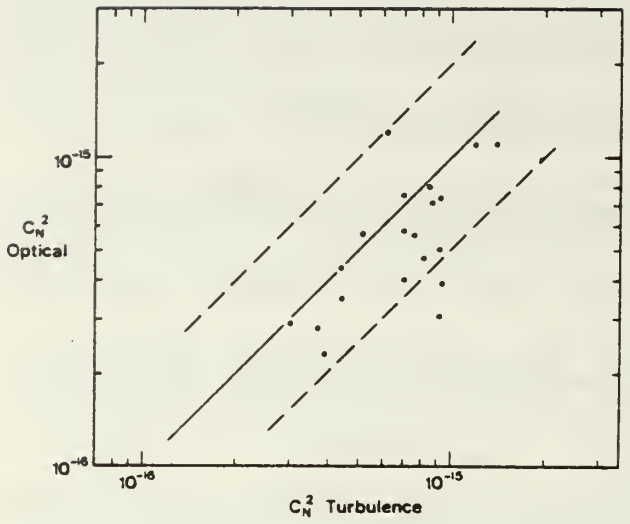

Figure 2 Refractive-index structure function, C_N^2, determined from direct optical measurement versus C_N^2 determined from microthermal point measurements of C_T^2 (Eq. 1) assuming C_Q^2 and C_{TQ} are negligible. The dashed lines represent factors of 2 disagreement.

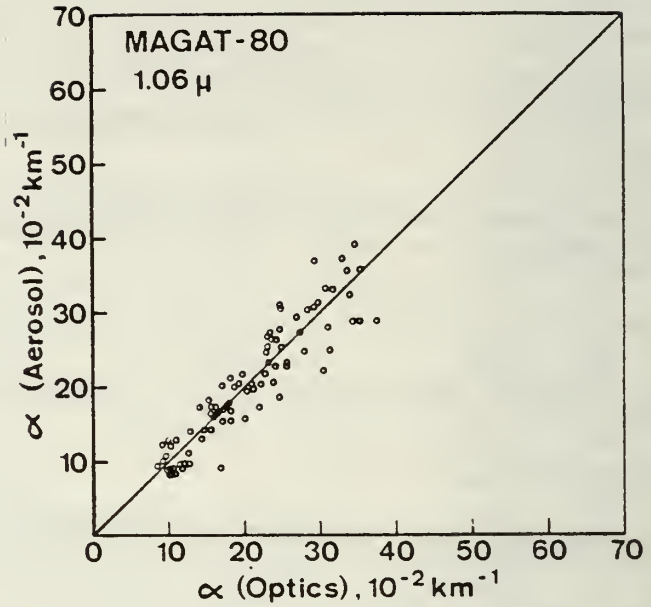

Figure 3 Aerosol extinction coefficient, α, determined from direct optical measurement versus α determined from point measurements of aerosol spectral density, N(r), and Eq. 2.

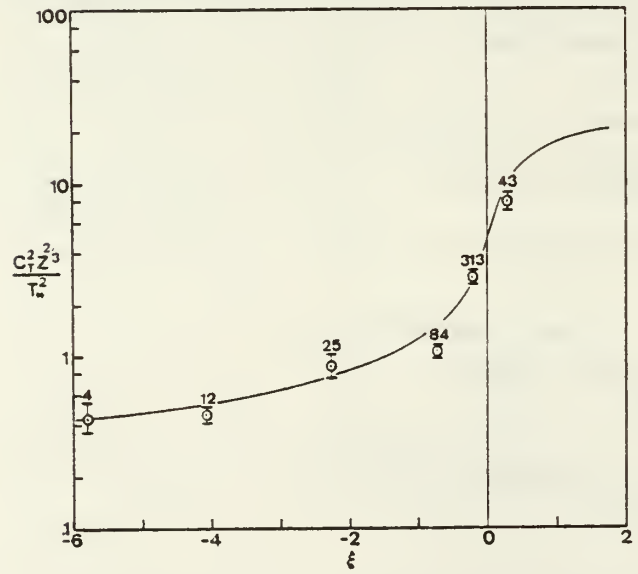

Figure 4a Dimensionless temperature structure function: overwater measurements (points) and overland empirical function[7] f(Z/L) (line).

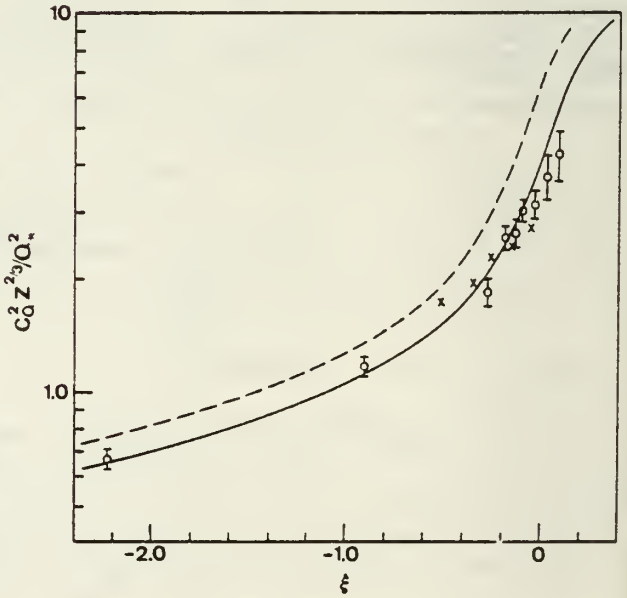

Figure 4b Dimensionless water vapor structure function: overwater measurements (points) and empirical function[7] A f(Z/L) (solid line).

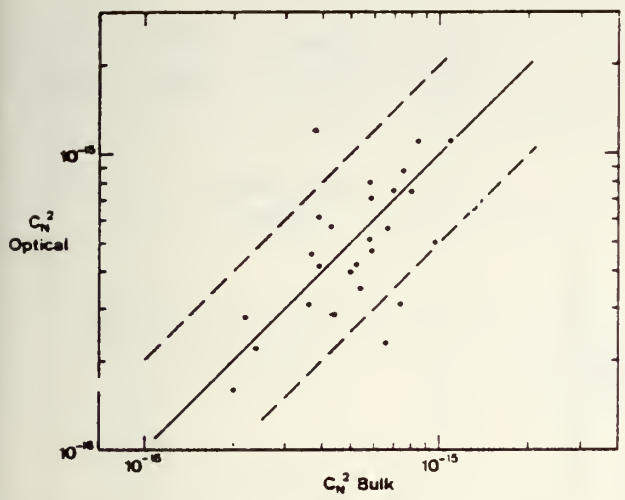

Figure 5 Similar to Figure 2 but the horizontal axis is C_N^2 determined from bulk model calculations (Eq. 1 and Eq. 3).

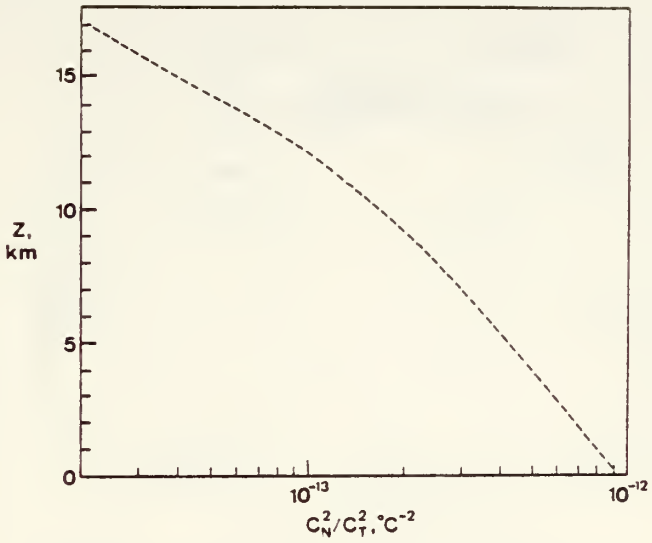

Figure 7 The ratio of C_N^2 to C_T^2 (neglecting the water vapor contribution) from Eq. 1 using the U.S. standard atmosphere.

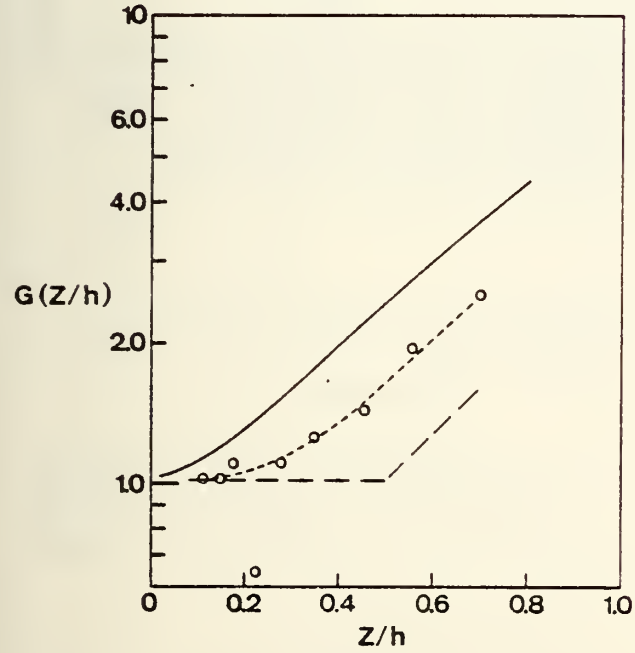

Figure 6 Average mixed layer dimensionless temperature structure function. The solid line is Frisch and Ochs[14] (h=300m). The dashed line is Kaimal et al[10] (h=1700m) and the points are from Fairall et al[15] (h=700m).

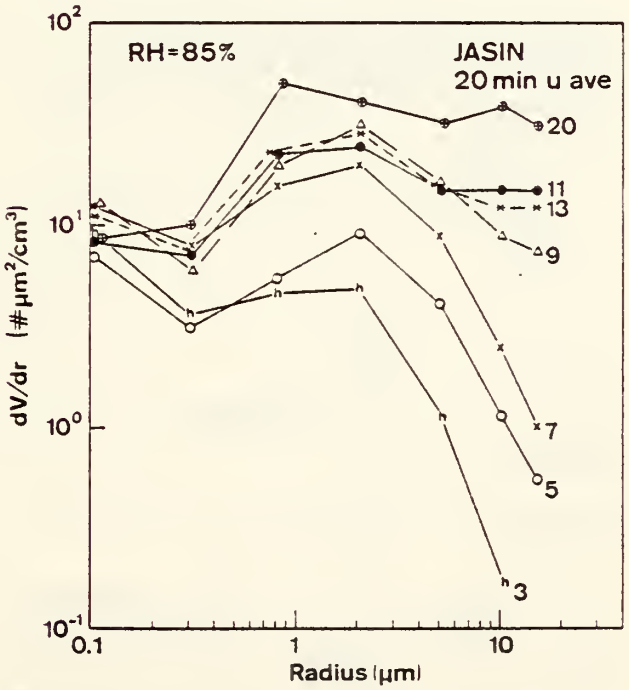

Figure 8 Ensemble average total aerosol volume spectra from JASIN. The number to the right of the spectrum is the wind speed category in m/sec.

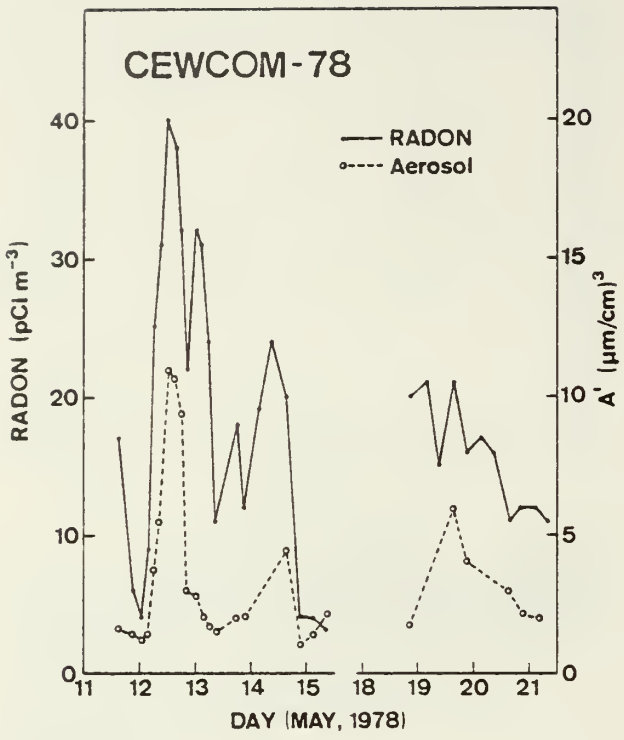

Figure 9 Time series of atmospheric ^{222}Rn activity (solid line, Larsen, Kasemir and Bressan[28]) and continental aerosol coefficient (dashed line), A.

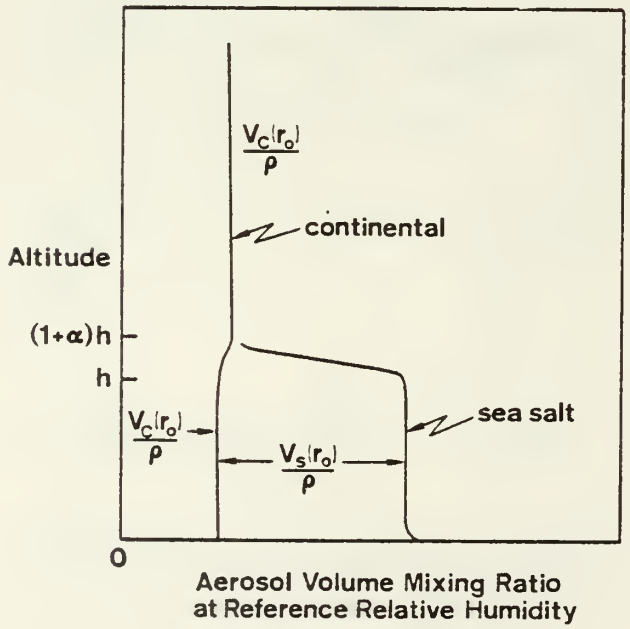

Figure 10 Schematic representation of the height dependence of continental (V_c) and sea-salt (V_s) aerosols at $S=S_o$.

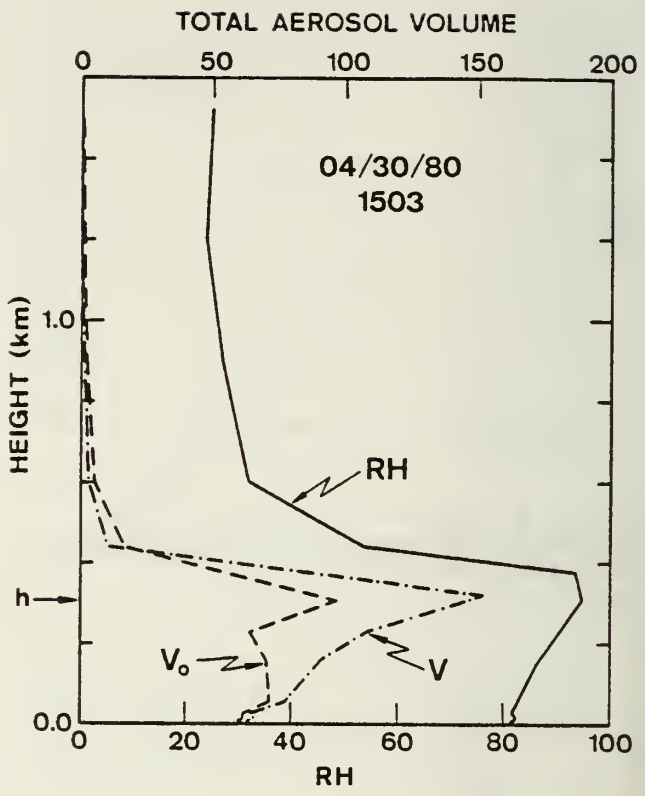

Figure 11 MAGAT aircraft measurements of the vertical profiles of relative humidity (RH), ambient aerosol total volume (V) and reference ($S=S_o$) aerosol total volume (V_o). The aerosol volume is in $\mu m^3/cm^3$.

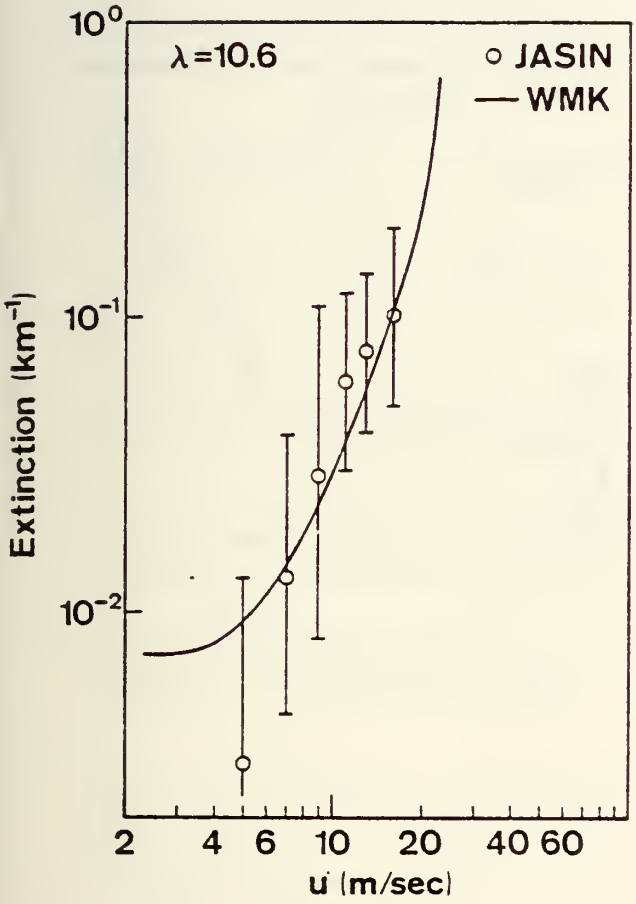

Figure 12 Aerosol extinction coefficient (circles) and WMK model predictions (line) at λ = 10.6 μm and RH = 87% as a function of 12 hour average wind speed.

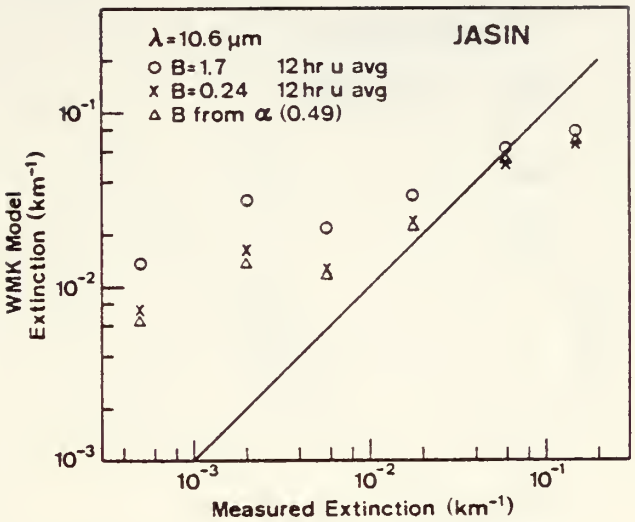

Figure 13 WMK model predictions of aerosol extinction at λ = 10.6 μm as a function of observed extinction (circles are B = 1.7, X's are B = 0.24 and triangle are B obtained from average correlation with visibility).

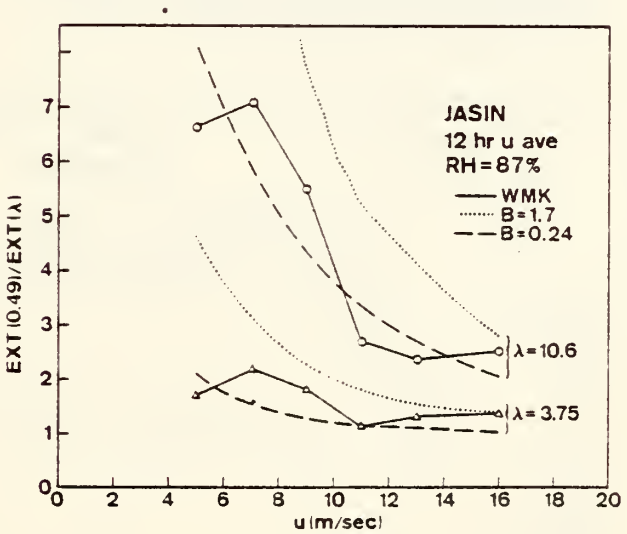

Figure 14 Ratio of aerosol extinction coefficient at λ = 0.49 μm to that obtained at λ = 3.75 μm and 10.6 μm. The circles are the JASIN data at λ = 10.6 μm, the triangles are the JASIN data at λ = 3.75 μm. The dashed line is WMK model with B = 0.24 while the dotted line is B = 1.7.

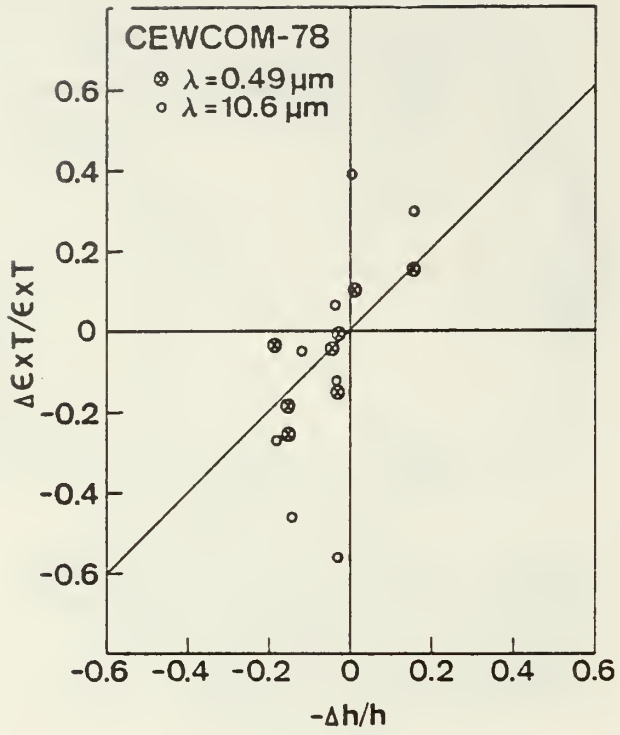

Figure 15 Fractional changes of aerosol extinction coefficient versus fractional changes in mixed layer height h for successive 4 hour periods.

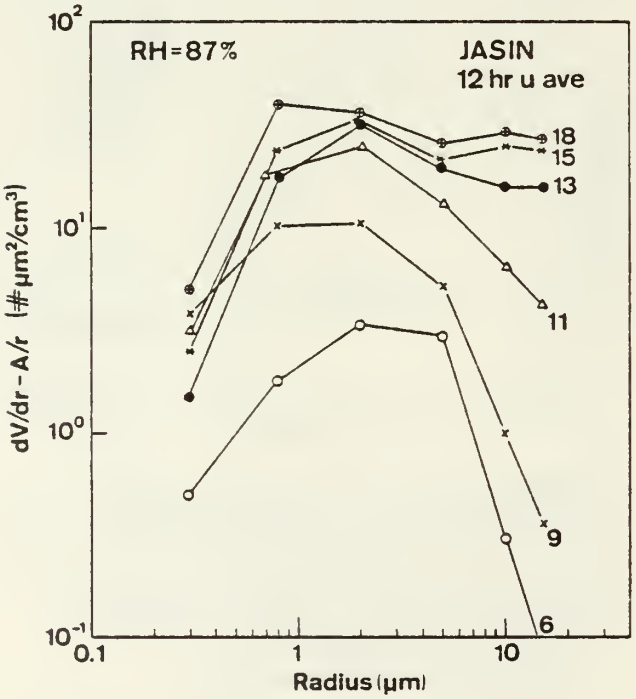

Figure 16 Ensemble average equilibrium sea salt volume spectra from JASIN. The number to the right of the spectrum is the wind speed category in m/sec.

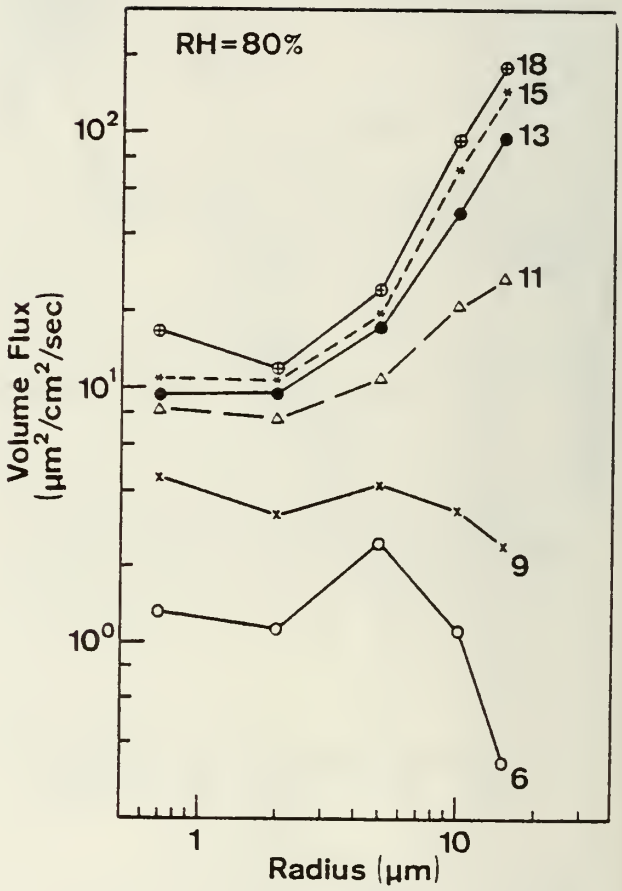

Figure 17 Ensemble average surface flux spectra deduced from Eq. 26. The number to the right of the spectrum is the wind speed in m/sec.

DISTRIBUTION LIST

		No. of Copies
1.	Defense Documentation Center Cameron Station Alexandria, Virginia 22314	2
2.	Library, Code 0142 Naval Postgraduate School Monterey, California 93940	2
3.	Dean of Research, Code 012 Naval Postgraduate School Monterey, California 93940	1
4.	Dr. C.W. Fairall BDM Corporation, 1340 Munras St. Monterey, California 93940	10
5.	Professor J. Dyer, Code 61Dy Naval Postgraduate School Monterey, California 93940	1
6.	Professor R.J. Renard, Code 63Rd Naval Postgraduate School Monterey, California 93940	1
7.	Assoc. Professor K.L. Davidson, Code 63Ds Naval Postgraduate School Monterey, California 93940	10
8.	Professor G.E. Schacher, Code 61Sq Naval Postgraduate School Monterey, California 93940	10
9.	Dr. A. Goroch Naval Environmental Prediction Research Facility Monterey, California 93940	1
10.	Dr. A Weinstein Director of Research Naval Environmental Prediction Research Facility Monterey, California 93940	1
11.	Dr. Richard Lipes Mail Stop 238-420 Jet Propulsion Laboratory 4800 Oak Grove Drive Pasadena, California 91103	1
12.	Dr. Kristina Katsaros Atmospheric Sciences Dept. University of Washington Seattle, Washington 98195	1

13. Dr. C.A. Friehe — 1
Deputy Manager for Research, RAF
National Center for Atmospheric Research
P.O. Box 3000
Boulder, Colorado 80307

14. Dr. J.C. Wyngaard — 1
CIRES
University of Colorado/NOAA
Boulder, Colorado 80309

15. Dr. Marvin L. Wesely — 1
Radiological and Environmental Research Divison
Argonne National Laboratory
Argonne, Illinois 60439

16. Dr. Owen Cote — 1
ESD/WE
Stop 7
Hanscom AFB, Massachusetts 01731

17. Dr. Hans Panovsky — 1
Department of Meteorology
Penn State University
State College, Pennslyvania

18. CDR K. Van Sickle — 1
Code Air-370
Naval Air Systems Command
Washington, D. C. 20360

19. Dr. A. Shlanta — 1
Code 3173
Naval Weapons Center
China Lake, California 93555

20. Dr. Barry Katz — 1
Code R42
Naval Surface Wespons Center
White Oak Laboratory
Silver Spring, Maryland 20362

21. Dr. J.H. Richter — 1
Code 532
Naval Oceans Systems Center
San Diego, California 92152

22. Dr. Lothar Ruhnke — 1
Code 8320
Naval Research Laboratory
Washington, D.C. 20375

23. Dr. Jost Businger 1
Atmospheric Science Dept.
AK 40
University of Washington
Seattle, WA 98195

24. Dr. Steven Burke 1
Naval Environmental Prediction Research Facililty
Monterey, CA 93940

25. Mr. Herb Hitney 1
Naval Ocean System Center
Code 532
San Diego, CA 92152

26. Mr. Paul Banas 1
Code 9220
Naval Oceanographic Office
NSTL Station
Bay St. Louis, MS 39522

27. LT Mark Schultz 1
Naval Environmental Prediction Research Facility
Monterey, CA 93940

28. Ted Zuba 1
Code Air-370
Naval Air Systems Command
Washington, D.C. 20360

29. Mr. Jay Rosenthal 1
Geophysics Division
Pacific Missile Range
Pt. Mugu, CA 93042

30. Dr. Michael J. Kraus 1
AFGL/LYS
Hanscom AFB, MA 01731

31. MAJ Bob Wright 1
AWS/DOOE
Scott AFB, IL 62225 1

32. MAJ Ed Kolczynski 1
AWS/SYX
Scott AFB, IL 62225

33. Joel S. Davis 1
Defense Sciences Div.
Science Applications, Inc.
1010 Woodman Dr., Suite 200
Dayton, OH 45432

34. L. Biberman 1
Institute for Defense Analysis
400 Army Navy Dr.
Arlington, VA 22202

35. Dr. Richard Gomez 1
DELAS-EO-MO
Atmospheric Sciences Laboratory
White Sands, NM 88002

36. Dr. R. Fenn 1
Air Force Geophysics Laboratory
Hanscom AFB, MA 02173